NUREG/CR-1313

Rationale for a Perturbation Method for Analyzing Fluid-Structure Interactions in BWR Pressure-Suppression Containment Systems

Prepared by P. W. Huber, K. M. Kalumuck, A. A. Sonin

Massachusetts Institute of Technology

Prepared for
U. S. Nuclear Regulatory
Commission

Available from

GPO Sales Program
Division of Technical Information and Document Control
U. S. Nuclear Regulatory Commission
Washington, D. C. 20555

and

National Technical Information Service
Springfield, Virginia 22161

NUREG/CR-1313
R4

Rationale for a Perturbation Method for Analyzing Fluid-Structure Interactions in BWR Pressure-Suppression Containment Systems

Manuscript Completed: January 1980
Date Published: February 1980

Prepared by
P. W. Huber, K. M. Kalumuck, A. A. Sonin

Department of Mechanical Engineering
Massachusetts Institute of Technology
Cambridge, MA 02139

Prepared for
Division of Reactor Safety Research
Office of Nuclear Regulatory Research
U.S. Nuclear Regulatory Commission
Washington, D.C. 20555
NRC FIN No. B6167

TABLE OF CONTENTS

Page

PART III: A PERTURBATION ANALYSIS OF FLUID-STRUCTURE INTERACTIONS IN A MODEL TEST SYSTEM

PART I

RATIONALE FOR A LINEAR PERTURBATION METHOD TO DEAL WITH THE FLOW FIELD PERTURBATIONS IN COMPLEX FLUID-STRUCTURE INTERACTION PROBLEMS*

Ain A. Sonin

Department of Mechnical Engineering
Massachusetts Institute of Technology
Cambridge, Ma. 02139

ABSTRACT

A formal justification is developed for a method in which hydrodynamic data for a transient in a rigid-wall system (derived, for example, from a small-scale experimental simulation) is used as input in a linear computation for the perturbation flow field due to actual wall flexibility. The method is useful in problems where the basic flow transient is so complex that it can be quantified only empirically, and where the fluid-structure interaction is too complex for the fluid side to be represented by à priori defined equivalent mass.

*Work supported by the U.S. Nuclear Regulatory Commission, Office of Nuclear Regulatory Research, Division of Reactor Safety Research, under Contract No. NRC-04-77-011.

1. INTRODUCTION

The analysis of loads resulting from complex flow transients in vessels is often further complicated by the effects of elastic boundaries. Numerical methods are almost invariably required, and even so, only relativley simple problems can be solved practicably [1]. The purpose of this paper is to identify a class of such problems where it is useful to separate the flow field into a component which would result if the walls were perfectly rigid, and a perturbation which arises because of wall flexibility. We will show rigorously that the effects of the wall flexibility can be derived separately by means of a perturbation analysis which in most cases is considerably simpler than the general problem. The pressure of the rigid-wall flow field appears as a forcing function at the boundary of the perturbation flow field.

This result is useful in two ways. First, it simplifies analysis. The calculation for the flow transient with assumed rigid boundaries can be done first and the additional effects of wall flexure can be derived by a separate perturbation calculation in which the fluid behaves linearly.

The second utility of our result arises in cases where the flow transient is so complex that a computation for it, or for its rigid-wall component, is difficult or impossible. In such cases, the first claculation can be replaced by experimental data for a small-scale simulation using rigid walls. Our analysis provides a formal justification for a method of using such data as

input in a relatively simple calculation for the perturbation caused by wall flexibility. Such a combined empirical/analytical approach is often more practical than a compiete empirical ismulation which includes both the effects of wall flexure and the fluid dynamic transient proper.

The technique of applying the experimental rigid-system load as a forcing function to compute structural oscillations has been used widely to solve problems involving flow-induced vibrations of cylinders and similar structures [2]. In those applications, the question of how one deals with the inertially induced pressure filed in the fluid is resolved simply by introducing an equivalent mass, one which can be determined semi-empirically for a given body geometry. The method we propose here is useful in more complex problems where an equivalent water mass cannot be specified à priori, and where a solution must be derived for the flow field perturbation which results from wall flexibility.

The method suggested here is not novel. Bedrosian [3], for example, has applied essentially this method to compute the fluid-structure interaction effects in pressure-suppression containment vessels of boiling-water reactors. The purpose of the present paper is to give the method a formal basis, and to specify the conditions which must be satisfied if it is to be valid.

2. ANALYSIS

We consider a class of problems where an essentially inviscid motion is induced in a liquid by the transient application of pressure at one or several of the places where the liquid is bounded by gas. Elsewhere, the liquid is bounded by solid, but flexible, walls. The general case is best illustrated with an example (Figure 1).

A vertical pipe is partially submerged in a liquid pool which is initially at rest, and bounded above by a region of gas. An event is triggered by a sudden discharge of gas or vapor into the pipe from above, causing the clearing of the liquid from the pipe, the formation of a gas bubble at the pipe end, and the rise or oscillation of the liquid in the pool. If the pool boundaries are rigid, the resulting pressure history at some point on the pool floor, for example, might be the one sketched in Figure 2. If the boundaries are elastic, they, and together with them the pool, would be set into oscillation, and the resulting pool acceleration and deceleration would give rise to an additional oscillatory component of pressure, as indicated on the figure. We aim to show how these two contribution to the pressure can be separated.

The liquid dynamics in governed by the equation of motion,

$$\rho \left(\frac{\partial \vec{v}}{\partial t} + \vec{v} \cdot \nabla \vec{v} \right) = -\nabla p - \rho g \nabla z , \qquad (1)$$

the quation of mass conservation,

$$\frac{\partial \rho}{\partial t} + \nabla \cdot (\rho \vec{v}) = 0 \qquad (2)$$

and the isentropic pressure-density relation, $dp/d\rho = c^2$. We shall assume that the latter applies in the linear approximation,

$$p - p_o = c_o^2 (\rho - \rho_o) \tag{3}$$

where p_o, c_o, and ρ_o are the pressure, speed of sound and density, respectively, in the undisturbed fluid.

The boundary conditions must be specified for Eqs. 1 - 3 at the free surfaces and at the solid walls. We assume that the pressure at any free surface is uniform and, for the purposes of the analysis of the liquid, given. In Figure 1, the trapped gaseous space above the liquid is one free surface, and the bubble emerging from the pipe is another. The free-surface boundary condition can thus be express as

$$p = p_i(t) \quad \text{at the i'th free surface.} \tag{4}$$

At the solid walls one must apply a boundary condition like

$$v_\perp = \frac{dx}{dt} \tag{5}$$

where $v_\perp$ is the fluid velocity component directed perpendicularly into the wall, and x is the displacement of the wall (away from the fluid) from its initial, equilibrium position under hydrostatic conditions. The wall displacement x is governed by a structural equation of motion which can be expressed symbolically as

$$m \frac{d^2x}{dt^2} = (p-p_o) - \sigma \left(x, \frac{dx}{dt}, \frac{d^2x}{dt^2}, \ldots, t\right) \tag{6}$$

where m is the local mass of the wall per unit area, p is the local instantaneous pressure in the fluid, p_o is the initial hydrostatic pressure, and σ is a local structural restraining force per unit area, whose magnitude depends on the displacement x of the wall from its initial equilibrium position, on the time derivatives of x, and possibly also on the time t itself. The form of σ is governed by structural considerations. Note that when the displacements x are small, the boundary condition embodied in Eqs. 5 and 6 can to a good approximation be applied at the equilibrium, or undisturbed, location of the wall rather than at the actual, instantaneous deflected position.

We separate the varibles into three components by writing

$$\vec{v} = 0 + \vec{v}_1 \ (\vec{r}, t) + \vec{v}_2 \ (\vec{r}, t) \tag{7}$$

$$p = p_o(\vec{r}) + p_1 \ (\vec{r}, t) + p_2 \ (\vec{r}, t) \tag{8}$$

$$\rho = \rho_o + \rho_1 \ (\vec{r}, t) + \rho_2 \ (\vec{r}, t) \tag{9}$$

where the subscript 0 refers to the values corresponding to the initial static conditions in the fluid, the subscript 1 refers to the hypothetical perturbation which would be caused if the imposed blowdown occurred in the system with rigid walls, and the subscript 2 refers to the remainder of the quantity, and represents the perturbation which can be attributed to the flexibility of the walls. The initial pressure distribution p_o is assumed to be hydrostatic,

$$p_o = \text{constant} - \rho_o g z \tag{10}$$

By definition, the rigid-wall flow is the solution of Eqs. 1-3 with $\vec{v}_2$, p_2 and ρ_2 equal to zero. Thus,

$$(\rho_o + \rho_1)\left(\frac{\partial v_1}{\partial t} + \vec{v}_1 \cdot \nabla \vec{v}_1\right) = -\nabla p_1 - \rho_1 g \nabla z \tag{11}$$

$$\frac{\partial \rho_1}{\partial t} + \vec{v}_1 \cdot \nabla \rho_1 + (\rho_o + \rho_1)\ \nabla \cdot \vec{v}_1 = 0 \tag{12}$$

$$p_1 = \rho_1 c_o^2 \tag{13}$$

where we used Eq. 10 to eliminate p_o, and assumed ρ_o to be constant. The boundary conditions for the rigid-wall solution are that

$$p_o + p_1 = p_i(t) \quad \text{at the i'th free surface} \tag{14}$$

and that

$$(v_\perp)_1 \equiv 0 \quad \text{at solid walls} \tag{15}$$

The equations for the perturbation (2) due to wall flexure is obtained by substituting Eqs. 7-10 into Eqs. 1 and 2, and subtracting Eqs. 11 and 12, respectively. One obtains the equation of motion

$$(\rho_o + \rho_1 + \rho_2)\left(\frac{\partial \vec{v}_2}{\partial t} + \vec{v}_2 \cdot \nabla \vec{v}_1 + \vec{v}_1 \cdot \nabla \vec{v}_2 + \vec{v}_2 \cdot \nabla \vec{v}_2\right) =$$

$$= -\nabla p_2 - \rho_2 g \nabla z - \rho_2 \left(\frac{\partial \vec{v}}{\partial t} + \vec{v}_1 \cdot \nabla \vec{v}_1\right) \tag{16}$$

and the mass conservation equation

$$\frac{\partial \rho_2}{\partial t} + \vec{v}_1 \cdot \nabla \rho_2 + \vec{v}_2 \cdot \nabla \rho_1 + \vec{v}_2 \cdot \nabla \rho_2 + \rho_2 \nabla \cdot \vec{v}_1$$

$$+ (\rho_0 + \rho_1 + \rho_2) \nabla \cdot \vec{v}_2 = 0 , \qquad (17)$$

and the pressure-density relation,

$$p_2 = \rho_2 c_0^2 \qquad (18)$$

Assuming that the wall flexure does not actually affect the gas pressure at the free surfaces, we can write the free-surface boundary condition as

$$p_2 = 0 \quad \text{at the i'th free surface} \qquad (19)$$

The boundary condition at the solid walls is

$$(v_\perp)_2 = \frac{dx}{dt} \qquad (20)$$

where x(t) is given by Eq. 6.

Eqs. 16 and 17 can be simplified considerably under conditions which are often not very restrictive in practice. Let

p_1 = typical amplitude of p_1

p_2 = typical amplitude of p_2

L = characteristic length over which gradients in velocity and pressure occur during the transient

τ_2 = characteristic time of the oscillation caused by wall flexure

x = typical wall displacement during wall flexure

We assume that

$$\frac{p_1}{\rho_o c_o^2} \ll 1 \tag{21}$$

$$\frac{p_2}{\rho_o c_o^2} \ll 1 \tag{22}$$

$$\frac{gL}{c_o^2} \ll 1 \tag{23}$$

$$\frac{\tau_2}{L}\sqrt{\frac{p_1}{\rho_o}} \ll 1 \tag{24}$$

$$\frac{x}{L} \ll 1 \tag{25}$$

The implication of these assumptions becomes apparent when we analyze the orders of magnitude of the various terms in Eqs. 11 and 12 and Eqs. 16 and 17.

We assume that the velocity v_1 arises from the acceleration of the liquid by a pressure difference p_1 acting over a distance L. The time of the acceleration is of order L/v_1. The order of magnitude of v_1 can then be estimated from the equation of motion as

$$v_1 \sim \sqrt{\frac{p_1}{\rho_o}} \tag{26}$$

The remaining order of magnitude estimates are self-evident:

$$\nabla \sim \frac{1}{L} \tag{27}$$

$$v_2 \sim \frac{X}{\tau_2} \tag{28}$$

$$\frac{\partial v_2}{\partial t} \sim \frac{X}{\tau_2^2} \tag{29}$$

$$\frac{\partial \rho_2}{\partial t} \sim \frac{\rho_2}{\tau_2} \tag{30}$$

In addition, Eqs. 13 and 18 give ρ_1 and ρ_2 in terms of p_1 and p_2, respectively.

Using these estimates, we are in a position to estimate the relative orders of magnitude of the various terms in the governing equation. We find that Eqs. 21 and 22 imply, first of all, that ρ_1 and ρ_2 are small compared with ρ_o. Eq. 21 also implies that the second terms in Eq. 12 is small compared with the third. Eq. 23 is equivalent to the assumption that the gravitational term in Eq. 11 is negligible compared with the pressure gradient term. Hence, the equations for the rigid-wall flow reduce in good approximation to.

$$\rho_o \left(\frac{\partial \vec{v}_1}{\partial t} + \vec{v}_1 \cdot \nabla \vec{v}_1\right) = -\nabla p_1 \tag{31}$$

$$\frac{\partial \rho_1}{\partial t} + \rho_o \nabla \cdot \vec{v}_1 = 0 \tag{32}$$

$$p_1 = \rho_1 c_o^2 \tag{33}$$

The boundary conditons for the rigid-wall flow are given by Eqs. 14 and 15.

On the left-hand side of Eq. 16, the second and third velocity terms are negligible compared with the time-derivative term when Eq. 24 applies, and the fourth term is neglibible when Eq. 25 applies. On the right-hand side of the same equation, the pressure-gradient term is large compared with the terms involving $\vec{v}_1$ when Eq. 21 applies, and also large compared with the gravitational term if Eq. 23 applies. In Eq. 17, the second and fifth terms on the left are small compared with the first when Eq. 24 applies. The third is small compared with the last one (the sixth) if Eq. 21 applies, and the fourth is small compared with the last one if Eq. 22 applies. Thus, the equations for the perturbation field caused by wall flexure reduce to

$$\rho_o \frac{\partial \vec{v}_2}{\partial t} = -\nabla p_2 \tag{34}$$

$$\frac{\partial \rho_2}{\partial t} + \rho_o \nabla \cdot \vec{v}_2 = 0 \tag{35}$$

$$p_2 = c_o^2 \rho_2 \tag{36}$$

The boundary conditions for this perturbation field are Eqs. 19 and 20. Consistent with the small-perturbation assumption, the free-surface boundary condition, Eq. 19, is to be applied at the free surface location obtained from the rigid-wall solution (or experiment), and the wall boundary condition, Eq. 20, is to be applied at the initial, undisturbed

wall location (which is the wall location in the rigid-wall solution). The displacement x(t) which appears in the boundary condition at the wall (Eq. 20) couples the perturbation field to the structural behavior of the wall. In the symbolic representation of Eq. 6, x(t) is governed by the equation

$$m \frac{d^2x}{dt} = p_1 + p_2 - \sigma \left(x, \frac{dx}{dt}, \frac{d^2x}{dt^2}, \ldots, t\right) \qquad (37)$$

Note that the equation 34-36 for the perturbation field do not themselves explicity involve the rigid-wall solution. The perturbation field due to wall flexure is coupled to the rigid-wall flow field only through the pressure p_1 which appears in the structural dynamic equation of the wall (e.g. Eq. 37) and through the instantaneous locations and shapes of the free surfaces (governed by the rigid-wall solution), where the boundary condition Eq. 19 must be applied. It is as if the rigid-wall pressure $p_1(t)$ appears as an externally applied transient pressure on the wall, and drives the wall (and fluid) oscillation calculated by the perturbation (2). Thus, if one has obtained, analytically or experimentally, the rigid-wall pressure distribution history p_1 at the walls and the time-dependent shapes of the free surfaces, one can apply the boundary conditions on the solution 2 and calculate the perturbations in velocity and pressure, throughout the fluid, caused by wall flexibility.

Eqs. 34-36 are the linearized acoustic equations for the liquid, and can be solved for example by the usual linear method of characteristics with the sound speed c_o taken as a constant. The liquid is, as it were, regarded somewhat as a "gel" with its free surface boundaries prescribed as a function

of time by the rigid-wall flow field. In the particular case where the period τ_2 of the wall oscillations is much longer than the acoustic transit time ℓ/c_o across the system, ℓ being the characteristic length of the liquid pool,

$$\frac{\ell}{\tau_2 c_o} \ll 1 , \tag{38}$$

Eqs. 34-36 reduce to the simple, linearized incompressible flow form

$$\rho_o \frac{\partial \vec{v}_2}{\partial t} = -\nabla p_2 \tag{39}$$

$$\nabla \cdot \vec{v}_2 = 0 \tag{40}$$

This constitutes a particularly simple case, since the pressure p_2 now satisfies Laplace's equation.

3. DISCUSSION OF APPLICATIONS

The analysis outlined here has an important application in the design of large vessels, such as the pressure-suppression containment systems of boiling-water reactors, where transient liquid flows are induced and wall flexibility effects must be accounted for. In many such cases the basic transient flow phenomena are very complex and can be quantified only by means of small-scale experimental simulation [4, 5]. Often it is impracticable to model both the effects of wall flexibility and the hydrodynamics on a small scale. The question then arises whether one can use the hydrodynamic data derived from small-scale tests with rigid walls, and derive from that the strains in the walls of a real, full-scale system where wall flexure may occur.

The present analysis gives a rigorous basis for such a procedure. Consider the situation in Fig. 1 as an example. Let us say we have available, from an experimental simulation with <u>rigid</u> walls, the pressure history $p_1(t)$ at every point on the walls and the locations of the free surfaces as functions of time. One can then obtain a numerical solution of the relatively simple, linear fluid equations, Eqs. 34-36 (or Eqs. 39-40, if Eq. 38 applies) for the perturbations caused by wall flexibility. The rigid-wall pressure $p_1(t)$ appears as a driving force in the wall boundary condition for the perturbation field (Eq. 20 and 37), applied at the initial undisturbed wall location, and the specified free surface locations define where the free surface boundary condition, Eq. 19, is to be applied.

The method is valid as long as the inequalities expressed in Eqs. 21-25 apply. The requirements expressed by Eqs. (21) - (23) are satisfied in most practical cases. In water, for example, it suffices that p_1 and p_2 be small compared with 2×10^4 bar, and that the characteristic length L of the flow transient be small compared with 2×10^2 km. Eq. (25) is also satisfied in many practical cases: it merely requires that the wall deflections x be small in amplitude compared with L.

The key requirement is Eq. (24). The characteristic length L is the length over which gradients in velocity and pressure occur in the fluid during the transient. Usually, this can be taken as the system size. The depth of the pressure suppression pool in a boiling water reactor, for example, is about 5 m. With L = 5 m and $p_1 \sim 1$ bar, Eq. (24) would be satisfed if the wall oscillation frequency is large compared with 2 Hz. A more conservative interpretation of the requirement would set L equal to the smallest characteristic flow length in the system. This would be of the order of 1 m in the example, and thus the conservative requirement in the example would be that the wall oscillation frequency should be large compared with 10 Hz.

REFERENCES

1. Belytschko, T., Nuclear Eng. and Des., 42 [illegible] 52. 1977.

2. Blevins, R. D., Flow-Induced Vibrati[illegible]strand Reihold Co., New York, 1977.

3. Bedrosian, B., private communication, 1978.

4. Sonin, A. A., and Huber P. W., and Sonin, A. A., J. Heat Transfer 601-604, 1978.

5. Anderson, W. G., Huber P. W., Sonin, A. A., J. Heat Transfer, 100, 605-612, 1978.

SYMBOLS

c	speed of sound in liquid
g	gravitational acceleration
L	characteristic length associated with gradients in velocity, density and pressure
m	wall mass per unit area
p	pressure
t	time
$\vec{v}$	velocity
v_1	component of velocity directed perpendicularly into wall
x	displacement of wall from equilibrium position, in perpendicular direction away from fluid
z	direction measured vertically upward, against gravity
ρ	liquid density
τ_2	characteristic time associated with the wall flexure (e.g. period of wall vibration).

Subscripts:

0	value corresponding to the initial conditions in the static fluid.
1	perturbation which would be caused if the event occurred in a rigid-wall system.
2	remainder of the quantity, i.e. additional perturbation caused by wall flexibility.

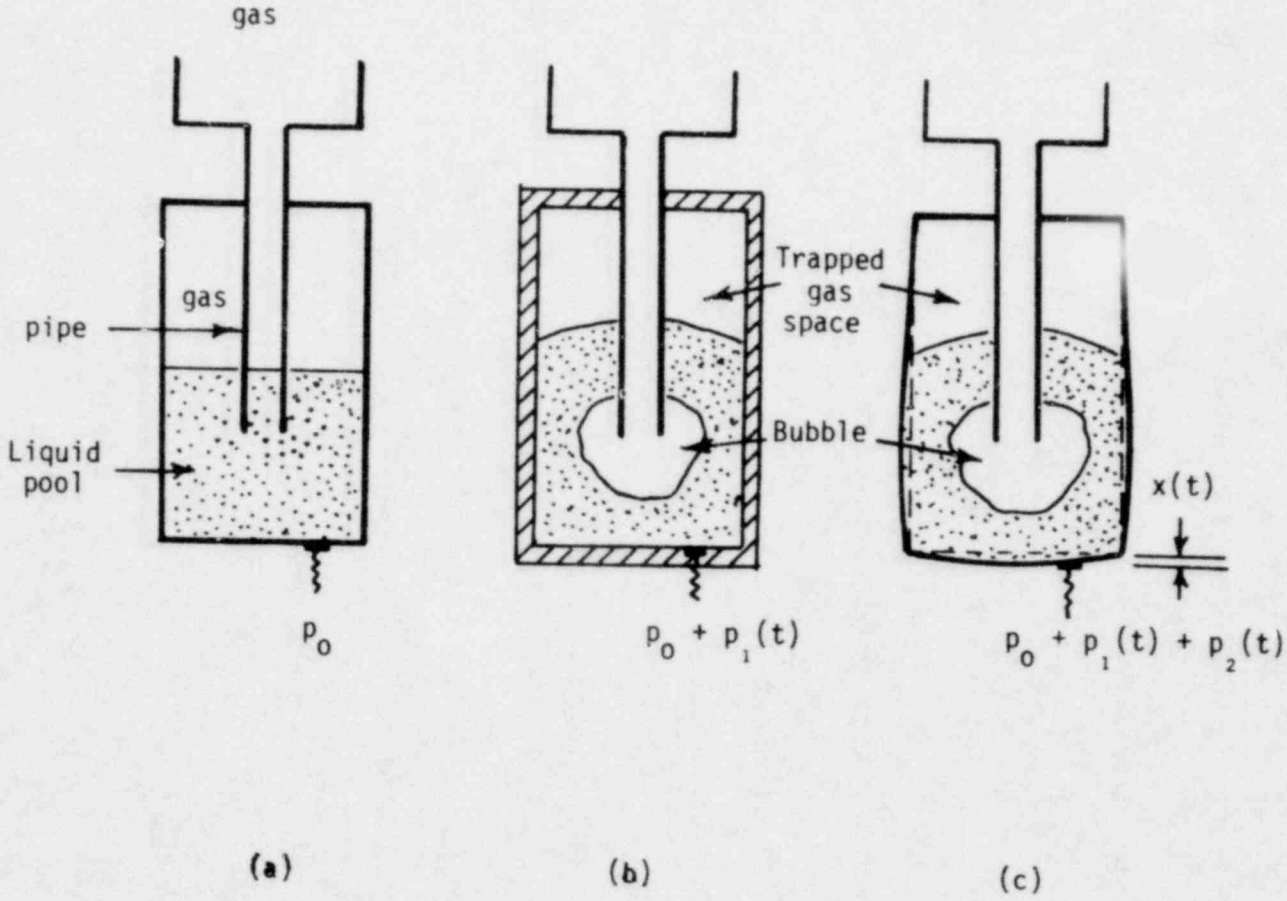

Figure 1: Example of flow transient. (a) Initial condition. (b) Time t in system with rigid walls. (c) Time t in system with flexible walls.

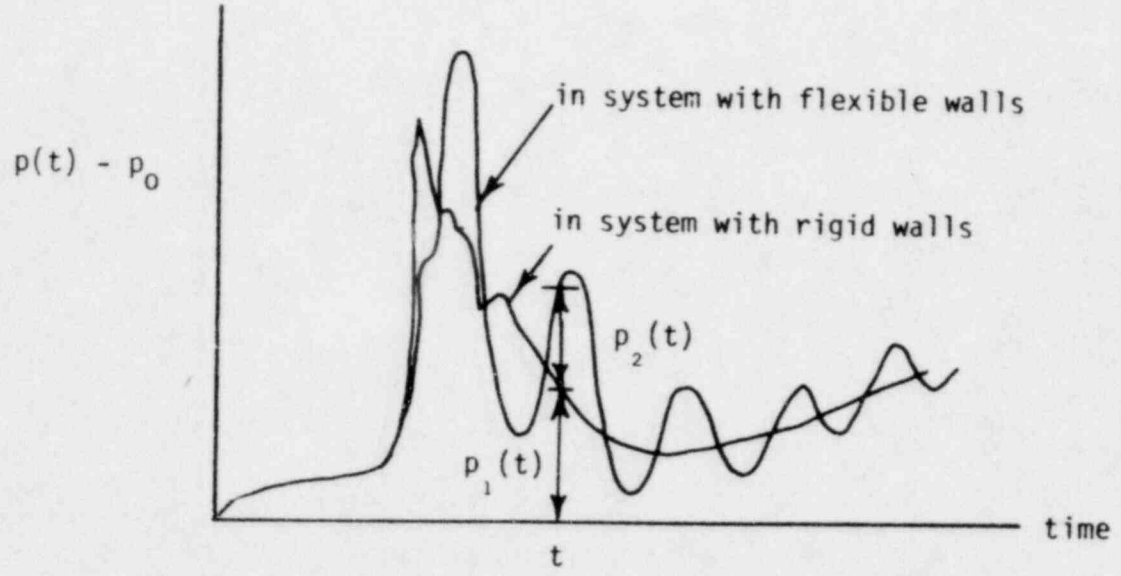

Figure 2: Sketch of pressure histories in rigid-wall and in flexible-wall systems.

PART II

A PERTURBATION METHOD FOR ANALYZING FLUID-STRUCTURE INTERACTIONS IN FLEXIBLE CONTAINERS PARTIALLY FILLED WITH LIQUID*

P. W. Huber, K. M. Kalumuck, A. A. Sonin

ABSTRACT

A perturbation method for analyzing the pressure fields developed when a complex hydrodynamic transient occurs in a liquid contained in a slightly flexible structure is outlined. The method involves a two step procedure in which the bulk liquid hydrodynamics are determined first, by analysis or experiment, and then used as an input to a calculation that predicts the perturbations to the pressure fields produced by structural flexibility. A treatment of the fluid-structure interface boundary conditions consistent with the assumptions underlying the perturbation method allows for the use of eulerian fluid equations and lagrangian structural equations. Criteria are presented for determining when the conditions of a specified problem lend themselves to this analytical approach.

*Work sponsored by the U.S. Nuclear Regulatory Commission, Office of Nuclear Regulatory Research under Contract No. 04-77-011.

1 Introduction

In this paper we discuss a class of fluid-structure interaction (FSI) phenomena with a combination of characteristics that distinguish it from most other FSI problems. Our analysis is motivated by problems involving complex hydrodynamic transients in vessels partially filled with liquid which arise in boiling water nuclear reactor containment systems, [1-5], in conventional power plant applications, and in the chemical process industry.

We consider a system (Figure 1, for example) consisting of a complex flexible structure partially filled with an incompressible liquid. Transient injection of a gas at one or more points produces a complex hydrodynamic transient in the liquid pool. The liquid experiences both bulk motion (driven by the rapid growth of one or more gas regions) and small displacement accelerations due to oscillation of the structure in response to the hydrodynamic excitation. In addition to the initial hydrostatic loading, two types of pressure loading are felt by the structure: the dynamic pressure due to the bulk fluid motion and the pressure arising from the relatively high frequency fluid acceleration associated with the structural response. Both pressures can be, in general, of the same order. Thus the liquid pressure fields can be significantly different from those that would be present if the structure were not flexible. The distinguishing feature of this class of FSI problems is that a hydrodynamic transient of arbitrary complexity is considered and significant liquid redistribution is allowed.

Analysis of problems of such complexity requires a numerical approach. Computer codes such as PELE-IC [6] attempt to solve for both the hydrodynamics and the FSI effects and employ separate fluid dynamics and structural dynamics algorithms. An iteration loop at each time step assures that the governing equations are satisfied for both the fluid and the structure and that continuity of pressure and velocity is satisfied at the fluid-structure boundary. Such schemes are costly in terms of both computer time and storage. These costs escalate rapidly with both the geometric complexity and the number of spatial dimensions that must be considered. In many FSI problems, an "added" mass distribution is computed for the fluid and used in conjunction with a structural dynamics algorithm. For transients such as those we consider, in which there is significant redistribution of the liquid, the added mass would have to be recalculated as the mass distribution changed. Similar comments can be made about the boundary integral or singularity method [7]. Analysis based on a modal superposition method is also difficult due to the change in system eigenvalves accompanying the liquid mass redistribution.

A promising analytical method that can supplement or serve as an alternative to existing analytical approaches is the "perturbation method" outlined in [8]. Under certain conditions, often satisfied in situations of practical interest, the FSI response can be modeled by this technique. The fluid flow fields are expressed as the superposition of components due solely to the strucutral oscillation and components due solely to the bulk fluid motion - the same components that would be present in an otherwise identical rigid walled

system undergoing an identical hydrodynamic transient. The analysis then becomes a two step procedure. The bulk fluid hydrodynamics are first determined by analysis and/or experimentation in a structurally rigid system. The results are then used as an input to a calculation which determines the perturbations caused by wall flexibility by solving a relatively simple set of equations which, in the fluid at least, are linear. This technique decouples the FSI effects from the bulk fluid motions. It does not decouple the fluid from the structure in as much as calculation of the perturbations involves simultaneous consideration of both the fluid and the structure. A concept similar to this is employed in [9] for coupling FSI effects to thermal-hydraulic effects.

The perturbation analysis simplifies the problem by enabling a full set of resources and specialized techniques to be devoted to one task at a time - resources that involve not only computer time and storage, but also development effort. The perturbation analysis can also make direct use of experimentally obtained hydrodynamic data - a capability of great utility when the analysis of the hydrodynamic transients alone is extremely complex.

In this paper we outline a perturbation method for analyzing incompressible FSI problems arising in flexible structures partially filled with liquid and undergoing complex hydrodynamic transients. Criteria for the applicability of this method are developed. In a companion paper [10] we demonstrate the implementation of this method for a laboratory test system and compare the predictions with experiment.

2 Fluid Domain Equations and Boundary Conditions

The perturbation equations in the fluid regions can be derived by a method similar to that of [8]. For an incompressible fluid the equation of motion and the equation of mass conservation are:

$$\rho\left(\frac{\partial \vec{v}}{\partial t} + \vec{v}\cdot\nabla\vec{v}\right) = -\nabla\,(P+\rho g z) + \mu\nabla^2\vec{v} \qquad (1)$$

$$\nabla\cdot\vec{v} = 0\ . \qquad (2)$$

We define:

$$P = P_0 + P_R + P_p \qquad (3)$$

$$\vec{v} = \vec{v}_R + \vec{v}_p \qquad (4)$$

where P_0 is the initial hydrostatic pressure, P_R and $\vec{v}_R$ are the pressure and velocity fields that would be developed in a completely rigid system, and P_p and $\vec{v}_p$ are the perturbation fields developed in an otherwise identical flexible structure. The fluid dynamics of the completely rigid system are, of course, also governed by equations (1) and (2) with

$$P = P_0 + P_R$$

$$\vec{v} = \vec{v}_R$$

If the equations obtained from the substitution of these expressions into equations (1) and (2) are subtracted from those obtained by substitution of expressions (3) and (4) into equations (1) and (2), the result is

$$\rho\left(\frac{\partial \vec{v}_p}{\partial t} + \vec{v}_R \cdot \nabla \vec{v}_p + \vec{v}_p \cdot \nabla \vec{v}_R + \vec{v}_p \cdot \nabla \vec{v}_p\right)$$

$$= - \nabla P_p + \mu \nabla^2 \vec{v}_p \qquad (5)$$

$$\nabla \cdot \vec{v}_p = 0 \qquad (6)$$

When the characteristic length and time scales for the hydrodynamics are much larger than the corresponding scales for effects due to structural flexibility, the three convective terms in (5) can be neglected compared to the temporal acceleration term yielding

$$\rho \frac{\partial \vec{v}_p}{\partial t} = - \nabla P_p + \mu \nabla^2 \vec{v}_p \quad . \qquad (7)$$

We discuss criteria for this simplification later. Equations (6) and (7) yield Laplace's equation for the perturbation pressure,

$$\nabla^2 P_p = 0 \quad , \qquad (8)$$

which lends itself to relatively straightforward, standard numerical solution techniques.

Fluid equations traditionally use an eulerian formulation while structural equations are usually cast in lagrangian terms. With appropriate treatment of the interface boundary conditions this distinction can be preserved in the simultaneous solution of the fluid and structural equations.

Figure 1 illustrates the various domains and their boundaries in a sketch of a liquid pool contained within a structure of circular cross section prior to a transient driven by the injection of air through two vertical pipes (Figure 1a) and during such a transient when the structure is completely rigid (Figure 1b). We identify a structural domain, a liquid domain $V_\ell(t)$, and gas domains $V_{gi}(t)$, $i = 1,\ldots,n$. Liquid-gas interfaces are denoted by $S_{\ell gi}(t)$. The initial wall-fluid interface, denoted by $S_{wf}(0)$, has a local outward lagrangian normal $\vec{n}_{wf}(0)$. Locations in any domain can be specified by use of an eulerian position vector $\vec{x}$ in a fixed reference frame. Thus $\vec{x}_{wf}(0)$ specifies the position of a point on $S_{wf}(0)$.

Figure 2a illustrates the deformation which occurs when the structure is flexible. This deformation is characterized by the difference between the location of the initial wall-fluid interface $S_{wf}(0)$ and the location of the wall-fluid interface at time t, $S_{wf}(t)$. Figure 2b, an enlarged local region depicts the change with time of $\vec{n}_{wf}$. It also introduces a lagrangian position

vector $\vec{u}$, which specifies the position at any given time of a particular particle of the structure. In general, $\vec{u}$ and its time derivatives will be part of the governing structure equations. The displacement of any point on the structure is implicitly a function of its initial position $x_w(0)$.

Coupling between the gas, liquid, and structure domains occurs through interaction at the various interface surfaces. Proper accounting for this requires continuity of velocity and (in the absence of surface tension) pressure across the interfaces.

Under the assumption (discussed later) that the liquid-gas interfaces $S_{\ell gi}(t)$ are not affected by wall flexure, the pressures in the gas regions are specified solely by the hydrodynamics and, therefore

$$P_p = 0 \quad \text{in } V_{gi}(t) \quad . \tag{9}$$

At $S_{wf}(t)$, continuity of velocity must be satisfied. Thus

$$\vec{v}(\vec{x},t) = \frac{\partial}{\partial t} \vec{u}\,(\vec{x},t) \text{ on } S_{wf}\,(t) \quad . \tag{10}$$

Using (4) and (10) and recognizing that $\vec{v}_R$ must be zero on $S_{wf}(t)$, we can write

$$\vec{v}_p(\vec{x},t) = \frac{\partial}{\partial t} \vec{u}\,(\vec{x},t) \text{ on } S_{wf}(t) \quad . \tag{11}$$

For small wall displacements, this boundary condition may be applied to the fluid domain at the initial wall-fluid interface $S_{wf}(0)$, a stationary surface:

$$\vec{v}_p(\vec{x},t) = \frac{\partial}{\partial t}\vec{u}_{wf}(\vec{x},t) \text{ on } S_{wf}(0) \qquad (12)$$

where

$$\vec{u}_{wf}(\vec{x},t) = \vec{u}(\vec{x}_{wf}(0),t) \qquad (13)$$

Solution of (8) requires that (12) be transformed from a velocity to a pressure formulation. In almost all applications the effects of viscosity on the perturbation motions can be neglected and equation (7) written as

$$\rho \frac{\partial \vec{v}_p}{\partial t} = - \nabla P_p \quad .$$

Taking the component of this equation normal to the wall and using equation (12) we arrive at a Neumann boundary condition

$$\rho \frac{\partial^2 \vec{u}_{wf}}{\partial t^2} \cdot \vec{n}_{wf}(0) = - \nabla P_p \cdot \vec{n}_{wf}(0) \text{ on } S_{wf}(0) \quad . \quad (14)$$

Thus the governing fluid equation (8) is solved in the region $V_\ell(t)$ bounded by the initial wall-fluid interface $S_{wf}(0)$ and the hydrodynamically determined liquid-gas interfaces $S_{\ell gi}$.

3 Applicability of the Perturbation Equations

We now discuss the physical implications of the assumptions made in deriving equation (8) and boundary conditions (9, 14). Criteria are developed in terms of order of magnitude estimates of various physically meaningful quantities to provide a measure of the accuracy of the perturbation method as applied to any particular problem. More quantitative verification and error estimation can be obtained by comparison of a test case with experiment or an otherwise known solution. A summary of the criteria derived below is presented in Table 1.

We defind a number of characteristic length and time scales:

L_R: characteristic hydrodynamic length over which gradients in velocity occur. Typically, this will be a liquid or gas region dimension.

L_λ: smallest characteristic wavelength of wall oscillation.

L_g: characteristic gas region dimension.

L_0: characteristic pool (fluid domain) dimension.

L_w: characteristic wall displacement during oscillation (estimated from the rigid system wall pressure histories and structural properties).

τ_R: characteristic hydrodynamic time (estimated from the bulk fluid motion in a rigid system).

τ_w: longest characteristic time for wall oscillation (estimated from the period of oscillation of the liquid filled structure).

τ_e: minimum excitation time constant (estimated from the rigid system wall pressure histories).

3.1 Incompressible Perturbations

The fluid perturbation equations model the perturbation flow fields as incompressible. Although the present derivation has also assumed the unperturbed (rigid structure) flow to be incompressible, this assumption is not necessary. It has been adopted here for the sake of brevity, and a derivation incorporating compressible effects in the unperturbed flow and resulting in equation (8) is possible [8]. It is quite possible for the driving hydrodynamic transient to include a component that introduces compressibility effects into the unperturbed flow while the structure oscillations introduce negligible compressible effects. The necessary criteria for neglecting compressibility effects in the perturbed flow are:

$$\left(\frac{L_0}{c_\ell \tau_w}\right)^2 , \quad \left(\frac{L_\lambda}{c_\ell \tau_w}\right)^2 << 1 \qquad (15)$$

where c_ℓ is the liquid speed of sound. The acoustic transit times through the liquid, L_0/c_ℓ and L_λ/c_ℓ must be small compared to the characteristic wall oscillation period τ_w.

3.2 Frequency of Wall Oscillations

The effects of nonlinear coupling between the convective accelerations associated with the unperturbed hydrodynamics and the perturbed flows will be small compared to the effect of the perturbation flow temporal acceleration provided the longest characteristic wall oscillation time τ_w is small compared to the shortest time τ_R characterizing the bulk fluid motions. The exact formulation of this criterion is two-fold:

$$\frac{\tau_w}{\tau_R}\,,\quad \frac{\tau_w}{\tau_R}\frac{L_R}{L_\lambda} \ll 1 \quad . \tag{16}$$

The factor of L_R/L_λ arises if gradients in $\vec{v}_p$ occur over a length L_λ when a different length L_R characterizes the unperturbed motions. The shortest time characterizing the hydrodynamically induced pressure transinets, τ_e, may be considerably shorter than the time associated with the bulk fluid motion (see 3.6 below). The time scales of relevance here are those associated with the liquid displacements, τ_R, which can be estimated from the hydrodynamics in a straightforward manner.

Estimation of τ_w is not as simple. Filling a structure with liquid can lower its natural frequency considerably. Rough estimates can be made by treating some significant fraction of the liquid mass as an added structural mass. Criterion (16) can, however, always be checked by performing a perturbation analysis and examining the calculated frequencies.

3.3 Amplitude of Wall Displacements

In order to neglect the nonlinear convective effects of the perturbation motions relative to the effects of perturbation flow temporal acceleration, the magnitude of L_w must be small compared to the shortest length scale L_λ over which gradients in perturbation velocity occur:

$$\frac{L_w}{L_\lambda} << 1 \quad . \tag{17}$$

Criteria (15, 17) lead to a linearized form of the fluid equation of motion. The other constraints imposed on L_w arise from consideration of the boundary conditions.

Application of boundary relation (14) assumes that the wall displacements are normal to the initial wall-fluid interface. The angle between $\vec{n}_{wf}(t)$ and $\vec{n}_{wf}(0)$ is of order L_w/L_λ. If

$$\frac{L_w}{L_\lambda} << 1$$

the displacements will be "quasi-normal" and will introduce only a small error. This criterion is the same as (17) and is thus satisfied whenever the linearized perturbation equation (7) applies. Perturbation analyses should therefore take advantage of this inherent boundary condition simplification.

All fluid domain boundary conditions are applied at the unperturbed boundary locations. This necessitates that

$$\frac{L_w}{L_0} << 1 \qquad (18)$$

in considering the wall-fluid interface boundary. Consideration of this approximation at the liquid-gas interfaces may require a geometry dependent modification to (18) depending on the shapes and sizes of the pool and gas regions, and on the structure modes and wavelengths of oscillation.

3.4 Inviscid Perturbations

In the formulation of the fluid boundary condition at a moving wall (14), viscous effects on the perturbation motions are neglected. This assumption is valid provided the product of the Reynolds and Strouhal numbers for the perturbation flow is much larger than unity:

$$\frac{\rho L_\Delta^2}{\mu \tau_w} >> 1 \quad . \qquad (19)$$

It should be noted that this is a constraint on the perturbations only and is not a limitation on the unperturbed (rigid structure) flows that can be analyzed.

3.5 Zero Gas Region Perturbation Pressure

The perturbation pressure at all liquid-gas interfaces is assumed to be zero. For this assumption to be valid, the gas perturbation pressures must be small compared to the liquid perturbation pressure at the wall-fluid interface. This is true when:

1. the pressures arising from fluid acceleration are much smaller in the gas than in the liquid and thus

$$\frac{\rho_g L_g}{\rho_\ell L_0} \ll 1 \tag{20}$$

where ρ_ℓ and ρ_g are the liquid and gas densities;

2. the transient perturbation pressures in the gas arising from compressibility effects are small and thus

$$\left(\frac{L_g}{c_g \tau_w}\right)^2 \ll 1 \tag{21}$$

where c_g is the speed of sound in the gas; and

3. the quasistatic equilibrium gas pressure changes are small. This requires that the changes in volume

of the gas regions are a small fraction of their unperturbed volumes or typically that

$$\frac{L_w}{L_g} << 1 \quad . \tag{22}$$

This criterion may be modified somewhat by such factors as geometry and the oscillation modes and wavelengths.

3.6 Excitation Time Constant

Flexible system responses having perturbations of large enough amplitude to be of interest arise when the system excitation has a period τ_e of the same or of smaller order than the system characteristic period τ_w [11] or when

$$\tau_e \lesssim \tau_w \quad . \tag{23}$$

Consideration of criteria (16, 23) shows that for the perturbation method to be both useful and applicable the rigid system must contain two characteristic time scales: one over which changes in bulk velocity occur, τ_R, and a much shorter time scale, τ_e, which excites the structural response. Examples of practical applications in which this occurs include the sudden injection of gas into a liquid or the condensation collapse of a steam bubble within a

liquid. Both cases involve changes in pressures in the pool that are much more rapid than the bulk pool displacements associated with them.

4 Treatment of the Structure

The traditional treatment of the fluid domain by an eulerian formulation and the structural domain by a lagrangian formulation can be preserved in a perturbation analysis by proper handling of the boundary conditions at the wall-fluid interface. Continuity of velocity leads to relation (14, [illegible]) which equates the eulerian fluid velocity at a stationary surface to the time derivative of a lagrangian structural displacement (12, 13). Continuity of pressure is achieved by equating the eulerian fluid pressure $(P_P + P_R)$ at a point $\vec{x}_{wf}(0)$ along $S_{wf}(0)$ to the loading in the lagrangian structural domain along $S_{wf}(t)$ at the point $\vec{u}_{wf}\ (\vec{x}_{wf}(0),t)$. The inclusion of P_R as part of the loading does not present a problem for decoupling the hydrodynamic and perturbation motions. It will appear in the structural equations as a forcing function [8] and is known in advance from separate calculations and/or experiment.

One simplification to the structural equation is neglecting the inertia of the structure relative to that of the liquid. This will be valid when the effective liquid inertia - or

"added mass" - is large compared to the structural inertia. The structural equations are then considerably simplified. The system can be thought of as moving through a series of quasistatic states. However, the transient oscillatory character of the FSI perturbation pressure fields will nevertheless be present.

5 Conclusions

The perturbation method is a powerful, practical tool for the analysis of the response of flexible structures partially filled with liquid undergoing complex hydrodynamic transients. It involves a two step procedure which requires the determination of the bulk hydrodynamics followed by a calculation of the induced FSI dynamics. This sequence of analysis permits an independent set of resources and specialized techniques to be exploited in each step. It admits the use of experimentally obtained data for the determination of the bulk fluid hydrodynamics. The treatment of the fluid-structure interface conditions allows the use of eularian fluid equations and lagrangian structural equations. The potential suitability of a perturbation analysis approach to any specified problem can be determined a priori by evaluating a number of defined, dimensionless groups.

REFERENCES

1 "Mark II Containment Lead Plant Program Load Evaluation and Acceptance Criteria," Nuclear Regulatory Commission Report NUREG-0487, October 1978.

2 Belytschko, T., "Methods and Programs for Analysis of Fluid-Structure Systems," Nuclear Engineering and Design, Vol. 42, 1977, pp. 41-52.

3 Collins, E. K., Lai, W., McCauley, E.W., and Pitts, J.H., "Final Air Test Results for the 1/5-Scale Mark I BWR Pressure Suppression Experiment," Lawrence Livermore Laboratory Report UCRL 52371, October 1977.

4 "Fluid-Structure Interaction 4-T Test Facility," Anamet Laboratories Report No. 1076.57-B, San Carlos, California, April 29, 1977.

5 Lu, S.C., Holman, G.S., and McCauley, E.W., "Effect of Torus Wall Flexibility on Forces in the Mark I BWR Pressure Suppression System -- Final Report," Lawrence Livermore Laboratory, October 1978.

6 McMaster, W.H., et al., "Coupled Fluid-Structure Method for Pressure Suppression Analysis," U.S. Nuclear Regulatory Commission Report NUREG/CR-0607, February 1979.

7 Krieg, R., "Coupled Problems in Transient Fluid and Structural Dynamics in Nuclear Engineering. Part 1: Safety Problems Solved by Flow Singularity Methods," Applied Mathematical Modelling, Vol. 2, June 1978.

8 Sonin, A.A., "Rationale for a Linear Perturbation Method to Deal with the Flow Field Perturbations in Complex Fluid-Structure Interaction Problems," U.S. Nuclear Regulatory Commission Progress Report, March 1979.

9 Shaaban, S.H., "Implicit 3-D Finite Element Solution to Fluid-Structure Interaction Induced by LOCA," Dynamics of Fluid-Structure Systems in the Energy Industry, ASME PVP-39, 1979, pp. 67-75.

10 Kalumuck, K.M. and Huber, P.W., "A Perturbation Analysis of Fluid-Structure Interactions in a Model Test System," (companion paper).

11 Harris, C.M. and Crede, C.E., editors, Shock and Vibration Handbook, Vol. 1, McGraw-Hill, New York, 1961, Chapter 8.

Table 1 Criteria for the applicability of the perturbation equations

Criterion	Section discussed in
(16) $\tau_w/\tau_R \ll 1$	3.2
(16) $\frac{\tau_w}{\tau_R}\frac{L_R}{L_\lambda} \ll 1$	3.2
(23) $\tau_e/\tau_w \lesssim 1$	3.6
(17) $L_w/L_\lambda \ll 1$	3.3
(18) $L_w/L_0 \ll 1$	3.3
(22) $L_w/L_g \ll 1$	3.5
(15) $(L_0/c_\ell\tau_w)^2 \ll 1$	3.1
(15) $(L_\lambda/c_\ell\tau_w)^2 \ll 1$	3.1
(21) $(L_g/c_g\tau_w)^2 \ll 1$	3.5
(19) $\rho_\ell L_\lambda^2/\mu\tau_w \gg 1$	3.4
(20) $\rho_g L_g/\rho_\ell L_0 \ll 1$	3.5

LIST OF FIGURES

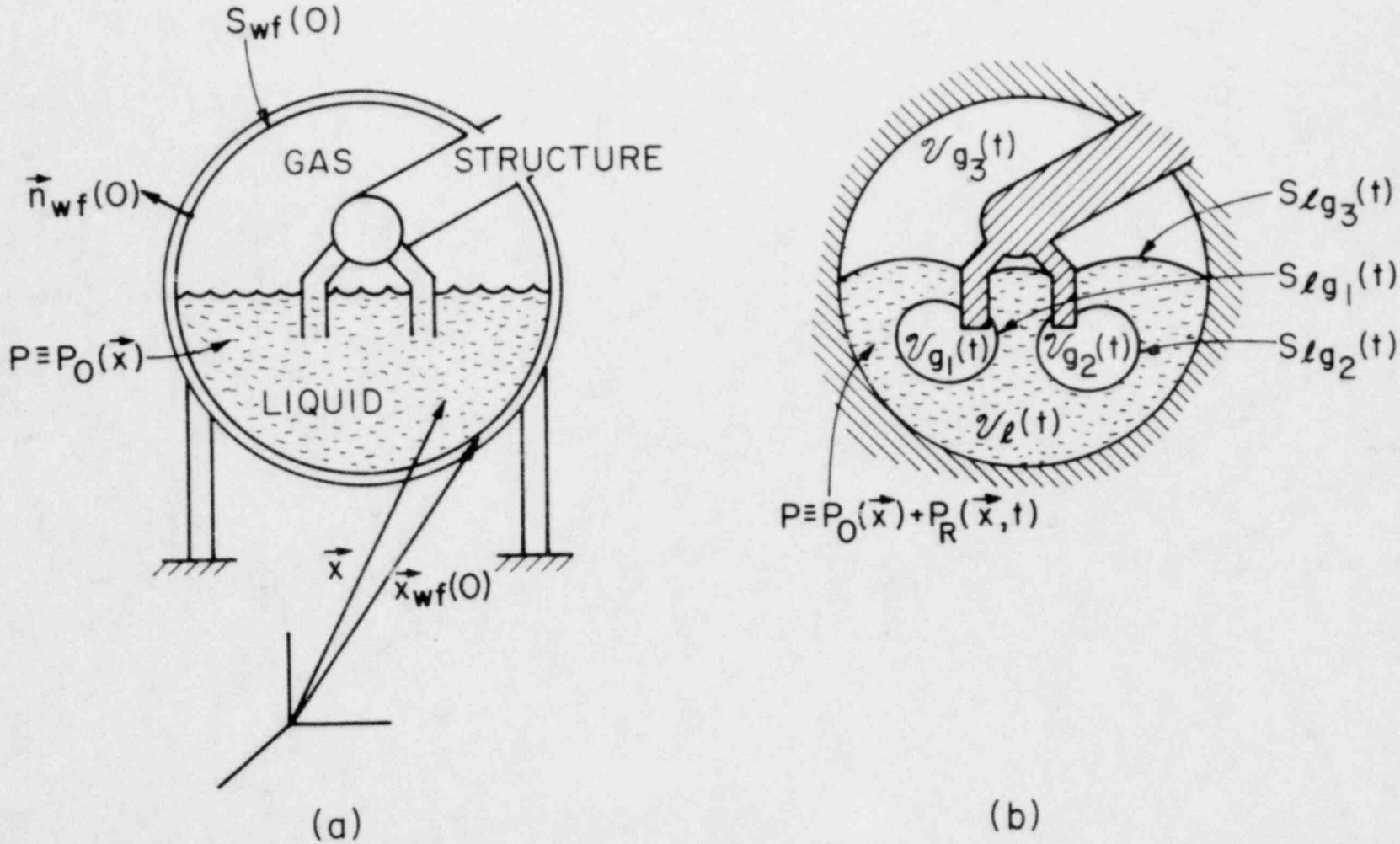

Figure 1 Features of a typical system of interest: (a) initially; (b) hydrodynamic transient in a system with rigid walls

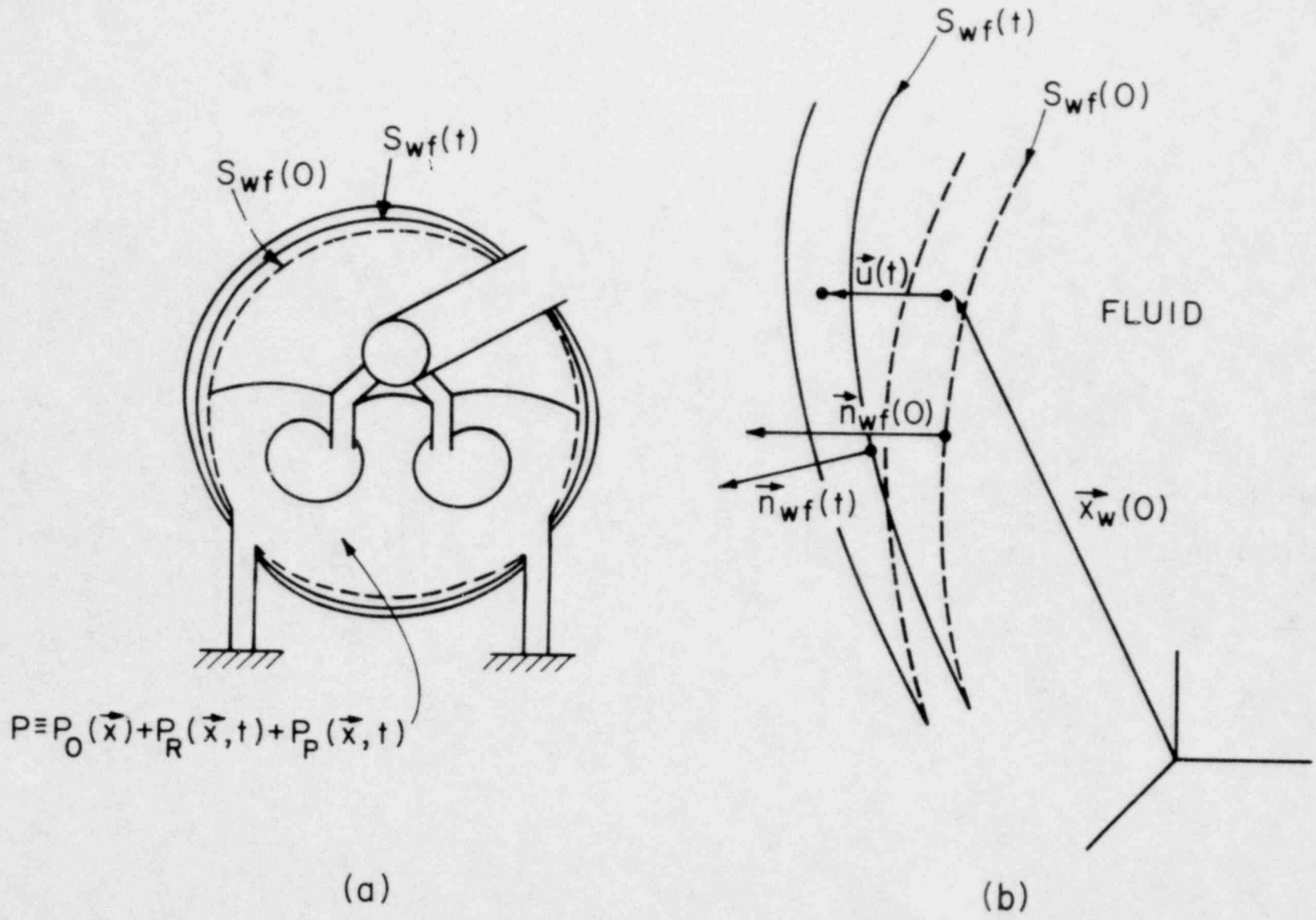

Figure 2 Hydrodynamic transient in a system with flexible walls: (a) system response; (b) enlarged local wall region

PART III

A PERTURBATION ANALYSIS OF FLUID-STRUCTURE INTERACTIONS IN A MODEL TEST SYSTEM*

K. M. Kalumuck and P. W. Huber

ABSTRACT

A perturbation analysis of fluid-structure interactions in a model test system of controlled flexibility excited by a complex hydrodynamic transient is presented. The analysis demonstrates the important features of the perturbation method and its implementation. Comparison of predictions with experiment provides a test of the analytical procedure and its underlying assumptions. The results illustrate the important effect of transient liquid mass redistribution on the flexible system response.

* Work sponsored by the U.S. Nuclear Regulatory Commission, Office of Nuclear Regulatory Research under Contract No. 04-77-011.

The authors wish to acknowledge the helpful discussions with Dr. Ain Sonin during the course of this work.

1 Introduction

The previous paper [1] outlines a preturbation method for analyzing the response of fluid filled flexible structures undergoing complex hydrodynamic transients and develops the criteria for the applicability of this method. In this paper we compare predictions based on perturbation method calculations with experimental results obtained in a simple test system. This paper has three purposes: to demonstrate the implementation of a perturbation method fluid-structure interaction (FSI) calculation in a simple system, to explore the basic physics of FSI in a system undergoing a complex hydrodynamic transient, and to provide one set of tests for verifying the numerous underlying assumptions of the perturbation method. The development of a general algorithm for modeling FSI phenomena was not one of our goals.

2 Summary of Experiments

Figure 1 shows a schematic of the cylindrical single downcomer test system partially filled with water in which our FSI experiments were conducted. Detailed descriptions of the test system, experimental procedure, and results have been documented elsewhere [2]. Only those experiments and results analyzed in this paper are summarized here. The test system's sidewalls and top are made of thick steel and are effectively rigid. The base consists of an interchangeable aluminum plate clamped at its periphery. Changing the base plate thickness

introduces different degrees of structural flexibility into the system. The rigid structure system characteristics are obtained by use of a 1.9 cm thick base plate. Sidewall taps enable pressure measurements to be taken at several stations in the liquid pool.

A hydrodynamic transient initiated by the opening of a fast acting valve is generated by injection of air from a large constant pressure reservoir or "drywell." The pressure beneath the plate is maintained constant at the initial pool surface pressure throughout the transient. The air injection forces the water out of the downcomer and forms a bubble that rapidly grows and redistributes the water in the pool causing the pool to "swell." Figure 2 shows the pool swell history traced from high speed film records in a geometrically similar rigid plexiglass system subject to a properly scaled but otherwise identical hydrodynamic transient initiated at $t = 0$. A dimensionless time $t^* = t\sqrt{g/2a}$, where a is the pool radius, has been defined in accordance with the hydrodynamic scaling laws for this system [3].

Typical pressure histories measured along the sidewall 5 cm above the base plate are presented in Figure 3 where the measured pressures have been nondimensionalized by the constant reservoir (drywell) pressure, P_D. The top oscillogram shows the rigid system pressure history containing a very rapid rise in pressure at the time the downcomer is cleared of water followed by a much more gradual change. The other three oscillograms show the measured pressure histories for plate thicknesses of 0.2, 0.16, and 0.1 cm [2].

3 Perturbation Method Analysis

3.1 Governing Equations

Figure 4 shows schematically the governing equations and boundary conditions used in implementing a perturbation method analysis for our test system. These follow directly from those outlined in [1]. The shaded liquid region, in which we ignore the presence of the downcomer, is bounded by four surfaces S_1, ...,S_4. The governing liquid region equation is:

$$\nabla^2 P_p = 0 \tag{1}$$

where P_p is the perturbation pressure. The free surface boundary condition is

$$P_p = 0 \quad \text{on } S_1, S_2 \tag{2}$$

where S_1 is the pool surface (approximated as horizontal throughout the transient) and S_2 is the bubble surface. The solid wall boundary conditions are:

$$\frac{\partial P_p}{\partial r} = 0 \quad \text{on } S_3 \tag{3}$$

$$\frac{\partial P_p}{\partial z} = \rho \frac{\partial^2 w}{\partial t^2} \quad \text{on } S_4 \tag{4}$$

where S_3 is the rigid sidewall, S_4 is the initial plate-fluid interface, z is measured vertically upward from S_4, r is measured radially outward from the center of S_4, w is the downward plate displacement from S_4, and ρ is the liquid density. A further

approximation is made here in neglecting the small plate deformation due to the initial hydrostatic loading. Hence, S_4 is taken as being perfectly flat. The displacement w shown in Figure 4 is exaggerated for clarity.

The governing equation and boundary conditions for the clamped circular base plate are:

$$D\nabla^4 w = P_R + P_p \quad \text{on } S_4 \tag{5}$$

$$w = 0 \text{ and } \frac{\partial w}{\partial r} = 0 \quad \text{at } r=a \tag{6}$$

$$\frac{\partial w}{\partial r} = 0 \quad \text{and} \quad D \frac{\partial}{\partial r} \nabla^2 w = 0 \text{ at } r=0. \tag{7}$$

Here D is the plate flexural rigidity and P_R is the hydrodynamically induced pressure in the rigid system. Experiments have shown P_R to be uniform over the base plate [4] -- varying only with time. In equation (5), the plate inertia has been neglected -- an assumption easily justified for our system by the much larger water inertia felt by the plate through P_p. The test system and imposed hydrodynamic transient are axisymmetric. This leads to boundary condition (7). Equation (5) enables the plate to be viewed as moving through a series of quasistatic states.

For solution of (5-7), a Green's function approach is adopted. The Green's function for this problem is found to be [5]:

for $b \leq r$,

$$\hat{w}(r,b) = \frac{1}{8\pi D}\left[\frac{(a^2-r^2)(a^2+b^2)}{2a^2} + (b^2+r^2) \ln \frac{r}{a}\right] ; \tag{8a}$$

for $b \geq r$,

$$\hat{w}(r,b) = \frac{1}{8\pi D}\left[\frac{(a^2-b^2)(a^2+r^2)}{2a^2} + (b^2+r^2)\ln\frac{b}{a}\right] . \qquad (8b)$$

Here b is the radial position of an arbitrary annular load. The plate displacement is then given by:

$$w(r,t) = \int_0^a 2\pi b[P_R(t) + P_p(r=b,z=0,t)]\,\hat{w}(r,b)db . \qquad (9)$$

The plate displacement is also related to the plate acceleration:

$$w(r,t) = \int_0^t \int_0^t \frac{\partial^2}{\partial t^2} w(r,t)\,dt\,dt . \qquad (10)$$

The complete set of equations to be solved then consists of the liquid (1) and structure (9) equations, boundary conditions (2-4), and identity (10). Coupling between the fluid and structure equations occurs through both boundary condition (4) and the loading in equation (9).

3.2 Computational Model

The technique adopted to solve the set of governing equations and their boundary conditions is a numerical time stepping one. A fully implicit second order accurate five-point finite difference scheme utilizing central differencing in an axisymmetric geometry as presented in [6] is used in the fluid domain. The radial derivatives are expanded prior to discretization. Appropriate forms of second order accurate boundary conditions are used. A detailed description of the scheme employed can be found in [7]. The finite difference

equations are solved in a two-dimensional time varying mesh. A typical mesh employed is shown in Figure 5. Two different axial mesh spacings are used such that the mesh point density is greater in the lower region of the pool than in the upper region. This provides a sufficient number of points between the bubble and the base plate to resolve the pressure gradient at the plate with reasonable accuracy. The number of mesh points varied with time from about 500 to 600. The location of each mesh point is fixed in time, but points are removed as the bubble grows and added as the pool rises. Mesh points are denoted by a pair of indices (i,j), i = 1,...,I; j = 1,...,J. The radial (r) and axial (z) mesh spacings are denoted by δr and δz such that $r = (i-1)\cdot\delta r$ and $z = (j-1)\cdot\delta z$. The derivative boundary conditions (3,4) are approximated by the introduction of a fictitious set of mesh points. The perturbation pressure $P^k_{i,j}$ at the point (i,j) and time step k (the subscript "p" being dropped for brevity) is set to zero for points that are along the pool or bubble surface or within the bubble. The equations corresponding to these points are removed prior to solution. The remaining set of fluid domain simultaneous equations can be expressed as

$$\underset{\sim}{A}\ \underset{\sim}{P}^k_p = \underset{\sim}{F}^k . \qquad (11)$$

Here, $\underset{\sim}{A}$ is a square, non-symmetric matrix containing the coefficients of the unknown $P^k_{i,j}$ arranged along five diagonals and is of order

$(I)\cdot(J-1)-N_B$ where N_B is the number of mesh points lying on the surface of or within the bubble. $\underset{\sim}{P}_p$ is a column vector whose elements are the unknown $P^k_{i,j}$. $\underset{\sim}{F}^k$ is a column vector which contains the inhomogenous terms of the mesh point equations. The equations comprising (11) are arranged in the order (1,1), ...,(I,1),...,(1,j),...,(i,j),...,(I,j),...,(1,J-1),...,(I,J-1).

The Green's function solution (9) to the plate equation is numerically integrated. In general, by selecting the radial locations of the plate nodes to correspond to those of the fluid mesh, one can express the downward displacement w_i at node i and time step k as

$$w_i^k = \sum_{\ell=1}^{I} C_{i,\ell}(P^k_{\ell,1}+P^k_R),\ i=1,\ldots,I \qquad (12)$$

where P^k_R is the value of P_R along the base plate at time step k. The expressions for $C_{i,\ell}$ depend upon the Green's function expression $\hat{w}$ (8) and the integration scheme. Investigation of the behavior of the product $b\hat{w}$ shows that it varies more rapidly with radius than does the load, $P^k_{i,1} + P^k_R$. Thus a Simpson's rule integration is performed over a much smaller interval than the mesh spacing (typically $\delta r/8$). Values of the perturbation pressure between mesh points are obtained by interpolation using a piecewise quadratic curve fit to the values of $P^k_{i,1}$. The interpolation weights are also accounted for in the values of $C_{i,\ell}$.

The displacement at node i is obtained from the acceleration history at that node from (10) using a double trapezoidal integration.

For zero initial displacement, velocity, and acceleration, this can be expressed at time $t = k\delta t$ (where δt is the time step size) as

$$w_i^k = \tilde{w}_i^{k-1} + \frac{1}{4}\,\delta t^2 \left(\frac{\partial^2 w}{\partial t^2}\right)_i^k, \quad i = 1,\ldots,I, \tag{13a}$$

where

$$\tilde{w}_i^{k-1} = \delta t^2 \sum_{\ell=1}^{k-1} (k-\ell)\left(\frac{\partial^2 w}{\partial t^2}\right)_i^{\ell} . \tag{13b}$$

Calculation of the flexible system response involves the simultaneous solution of four sets of linear algebraic equations: the fluid finite difference equations (11), the plate displacement equations (12), relation (13), and a discretized form of equation (4) which can be expressed as

$$\left(\frac{\partial p}{\partial z}\right)_{i,1}^k = \rho \left(\frac{\partial^2 w}{\partial t^2}\right)_i^k . \tag{14}$$

These equations are reduced to a single system of equations by combining (12) and (13) and substituting the result by use of (14) into $\underset{\sim}{F}^k$ of (11). The resulting expression for $\underset{\sim}{F}^k$ is a function of $\underset{\sim p}{p^k}$. Rearrangement of this set of equations leads to a new set of equations to be solved for the unknown perturbation pressures:

$$\underset{\sim}{A}^{*k}\ \underset{\sim p}{p^k} = \underset{\sim}{F}^{*k} . \tag{15}$$

The elements of $\underset{\sim}{F}^{*k}$ are given as

$$F^{*k}_m = 8\rho \frac{\delta z}{\delta t^2} \left(P^k_R \cdot \sum_{\ell=1}^{I} C_{m,\ell} - \tilde{w}^{k-1}_m\right), \quad m = 1,\ldots,I$$

$$F^{*k}_m = 0, \quad m > I \ . \tag{16}$$

The elements of A^{*k} are given by $A^{*k}_{m,n} = A^k_{m,n} + C_{m,n}$ when both $m \leq I$ and $n \leq I$ and by $A^{*k}_{m,n} = A^k_{m,n}$ whenever $m \geq I$ or $n \geq I$.

The matrix $\underset{\sim}{A}^{*k}$ is banded with a bandwidth of $2I + 1$. The presence of nonzero elements arising from the $C_{m,\ell}$ expressions precludes a solution by a block tridiagonal algorithm. A standard banded matrix solution routine was used to solve equation (15) for $\underset{\sim}{p}^k_p$ at each time step.[1] We did not attempt to develop a more efficient solution algorithm that would take advantage of the many zero elements within the band of $\underset{\sim}{A}^{*k}$. After $\underset{\sim}{p}^k_p$ is found from (15), w^k_i and $\left(\frac{\partial^2 w}{\partial t^2}\right)^k_i$ are found from equations (12-14).

It is interesting to note a possible interpretation of the effect of equations (12-14) on the fluid equations (11). Using these equations, the pressure gradient normal to the plate can be expressed as:

$$\left(\frac{\partial p}{\partial z}\right)^k_{i,1} = \rho \frac{4}{\delta t^2} \left(\sum_{\ell=1}^{I} C_{i,\ell}\, p^k_{\ell,1} + P^k_R \cdot \sum_{\ell=1}^{I} C_{i,\ell} - \tilde{w}^{k-1}_i\right). \tag{17}$$

---

[1] LEQT1B from the International Mathematical and Statistical Libraries, Inc. -- "IMSL."

The term $\tilde{w}_i^{k-1}$ is known from the history of the plate motion and does not depend on any quantities at time step k. At any time step, then, all unknown quantities are expressed in terms of the perturbation pressure field. The structure can be viewed as imposing a special type of boundary condition or constraint on the fluid: the normal perturbation pressure gradient at any point of the plate-fluid interface is a function of the pressure at every point of the interface (17). This is simply the result of the boundary integral nature of the problem.

Due to the fully implicit nature of the solution algorithm, the time step size is not limited by a stability criterion. It is limited, however, by a resolution requirement. That is, δt must be small enough to adequately resolve the expected frequencies of oscillation. With this in mind, δt was selected such that a minimum of about eight time steps occurred within the experimentally observed oscillation period.

The liquid configuration as a function of time is an input to the model. The bubble is approximated as an ellipsoid with three parameters fit by trending from the observed bubble history (Figure 2). The boundary is further approximated by taking it to lie along the mesh lines which are closest to the computed boundary. The change in the location of the pool surface is computed from continuity once the change in bubble volume is known and is also approximated to lie along a mesh line. A comparison of approximated bubble shapes and pool heights with those observed is shown in Figure 6 for three selected times.

Also input to the model is the experimentally determined rigid system base plate pressure history ($P_R(t)$ in equation (9)) and the rigid system pressure history at all other locations at which the flexible system response is desired. With this information, the complete perturbation pressure field is calculated at each time step. The predicted flexible system pressure is then the sum of the computed perturbation pressure and the rigid system pressure at the location of interest.

4 Perturbation Method Predictions and Comparison with Experiment

The predicted flexible system perturbation pressure amplitudes vary significantly throughout the pool. Figure 7 shows the predicted 0.2 cm flexible base plate system pressure history nondimensionalized by P_D at two sidewall locations and two base plate locations. The 0.1 cm base plate case exhibits similar behavior. The peak value of the flexible system pressure varies by about a factor of 2.5 between stations (a) and (d) of Figure 7. The perturbation pressures are largest at the base plate and decrease to zero at all liquid-gas interfaces. In Figure 7d the line of zero absolute system pressures dip below this value several times in the central region of the plate. This suggests the possibility of some cavitation occurring in the experimental tests which has not been investigated experimentally nor accounted for in our model. The maximum predicted flexible system pressure at the plate center represents an overshoot of about 50% when compared to the rigid system plate pressure.

Figure 7 also shows that the predicted perturbation pressure amplitudes decay after their first peak at rates which vary throughout the pool. That a decay should be predicted at all is at first surprising since the model does not account for structural damping or fluid viscosity. The decay is, in fact, the result of the liquid redistribution driven by the bubble growth. Otherwise identical calculations conducted without a growing bubble exhibited no perturbation decay.

Figures 8 and 9 show the predicted perturbation pressure distributions at two selected times. They illustrate the change with time of this distribution and thus the relative importance of the perturbations in various regions of the pool. The figures also include the predicted flexible system response and measured rigid system pressures along the sidewall at $z/a=0.7$ and $z/a=1.7$. The predicted flexible system pressures at the instants of time at which the P_p isobars are calculated are indicated by arrows on the pressure histories. In the region of the pool at elevations less than that of the bubble, the perturbation pressures are large (of the same order as the rigid system pressures) and decrease with elevation roughly linearly. At elevations at or above that of the bottom of the bubble they are much smaller. Thus it appears that there are two regions of influence within the pool: one beneath the bubble and relatively near the plate in which FSI effects are important and a second near and above the bubble in which the influence of the plate oscillation is much less. As the bubble grows, its region of influence grows and the large amplitude perturbation isobars

($\left|\frac{P_p}{P_D}\right| \gtrsim 0.1$, say) move closer to the plate. Such behavior leads to the predicted decay in perturbation amplitudes. (In comparing the magnitudes of P_p/P_D in Figures 8 and 9, it must be remembered that these figures represent different times in the oscillation cycle.)

Model pressure history predictions on the pool sidewall at $z/a = 0.7$ are compared with experiment for the cases of a 0.1 cm and a 0.2 cm thick base plate in Figures 10 and 11. A brief comparison of the predicted frequency content, peak pressures, and decay rates with those experimentally observed is presented in Table 1. Values of the per cycle decay rates, d, are calculated from the formula:

$$P_{p,n} \equiv P_{p,0}(1-d)^n \qquad (18)$$

where n is the number of cycles considered, $P_{p,0}$ is the amplitude of the perturbation pressure at the beginning of the first cycle considered, and $P_{p,n}$ is the amplitude n cycles later. The agreement is generally good. The initiation of a large amplitude decaying oscillation at the "spike" in the rigid system pressure history is clear in both calculations and experiment. For both plate thicknesses, an increase in perturbation frequency is predicted and observed experimentally. For both plates, the predicted frequencies are somewhat lower than observed experimentally (25 - 30% low for the 0.1 cm plate and 15 - 20% low for the 0.2 cm plate). For the 0.1 cm plate the model predicts a slight (2%) undershoot in comparing the peak value of the flexible system pressure history to that of the rigid system while an overshoot of about 21% is

observed experimentally. The model predicts an overshoot of about 6% for the 0.2 cm plate which agrees well with experiment. The predicted model decay rates are somewhat low but comparable to those observed.

Model predictions at z/a=1.7 are compared with experiment for the 0.2 cm plate case in Figure 12. Both the measured and predicted flexible system pressure histories differ little from the rigid system history. They exhibit minor perturbations shortly after the rigid system history peak and essentially no perturbations at later times.

5 Discussion

Our calculations and comparisons with experiment illustrate the essential features of a perturbation method FSI analysis and demonstrate both the simplicity and promise of this method. Relatively few refinements have been implemented in our calculations primarily because the agreement between prediction and experiment is near the level of experimental repeatability [2,4]. The comparisons presented here are not intended to be an exhaustive verification of the perturbation method, but rather to provide one systematic test of the procedure and its underlying assumptions. Our predictions illustrate the important effect that liquid mass redistribution has on both the frequency content and the amplitude of the flexible system's pressure fluctuations. The analysis and results can be contrasted to those of a lumped parameter model [2] which requires prior specification an "effective" pool depth (or "added liquid

mass") and is unable to predict any detailed FSI response features.

The criteria for the applicability of the perturbation method are evaluated for our test system in Table 2 where ρ_ℓ and ρ_g are the liquid and gas densities, c_ℓ and c_g are the speeds of sound in the liquid and gas, and μ is the liquid viscosity. Characteristic length and time scales used are defined as [1]:

L_R: hydrodynamic length over which velocity gradients occur.

L_λ: smallest wall oscillation wavelength.

L_g: gas region dimension.

L_0: pool (fluid domain) dimension.

L_w: wall displacement during oscillation (estimated from the rigid system pressures).

τ_R: hydrodynamic time (estimated from the rigid system bulk fluid motion).

τ_w: longest period for wall oscillation.

τ_e: minimum excitation time constant.

The length scales L_R, L_λ, L_0, and L_g are all taken to be the plate diameter. Both τ_R and τ_e are estimated from the rigid base plate pressure history. Table 2 shows that all criteria are easily satisfied except for (2) for the 0.1 cm base plate system. Thus the perturbation method assumptions should introduce negligible error with the possible exception of some nonlinear coupling effects between the perturbed and unperturbed motions not being accounted for in the analysis of the 0.1 cm plate system.

In developing a model for our test system we have made several additional assumptions not central to the perturbation method. Omission of the downcomer should introduce negligible error. It is partly enclosed by the air bubble and is in a region of very small $|P_p|$. The approximation of the pool surface as flat and horizontal (neglecting the growth of irregular pool surface instabilities; see Figure 2) should be of minor importance for similar reasons. The initial static plate deflection due to the weight of the water is an order of magnitude less than those during pool swell and is easily neglected.

The better agreement between prediction and experiment for the 0.2 cm plate than for the 0.1 cm plate may be largely due to plate tension effects which have been neglected in the model plate equation. Neglecting tension relative to bending stress for a circular clamped plate of thickness h deforming under a uniform load q will introduce an error that can be estimated from [8]:

$$\frac{q\,a^4}{64\,Dh} = \frac{w_{max}}{h} + \frac{1+\nu}{2}\left(\frac{w_{max}}{h}\right)^3 \qquad (19)$$

where w_{max} is the maximum plate displacement and ν is Poisson's ratio. The first term on the right-hand side of (19) is due to bending and the second is due to tension. If we take q to be the maximum value of P_R on the plate, the estimated errors are 21% and 0.2% for plate thickness of 0.1 cm and 0.2 cm, respectively. Since tension stiffens the plate, its inclusion in the model would increase the predicted frequencies -- enhancing agreement with experiment for the thinner plate. Modification of the predicted peak pressure overshoot should also occur.

The input data -- bubble shape and size, P_R on the plate, and P_R at various sidewall locations -- were obtained from several different experimental runs, and model predictions are compared to data from yet other runs. To compensate for experimental variability, the time coordinates of the data were shifted a small amount so that they would be equivalent in each set of data. Typically this shift was less than 2% of the total time period under consideration ($t^* < 0.01$) -- well within the bounds of experimental variability [4].

To save computation time, the liquid configuration was changed at each time step only during the initial period of bubble growth. At later times ($t^* \gtrsim 0.25$), the liquid configuration was modified every fifth time step for the 0.2 cm plate system. Thus the input bubble growth lags the experimental records. This results in a maximum error of about 6% in bubble "radius." Such an underapproximation of bubble size will lower the predicted perturbation frequencies and decay rates.

The run to run experimental initial liquid depth variation was about 2% [2]. The initial liquid depth used in the calculations is about 6% higher than the nominal experimental value. This should result in a prediction of frequencies that are about 3% low.

Based on simple tests of our algorithm we believe the errors introduced by the numerical schemes to be at most of the same order as the other uncertainties discussed above. As described earlier, provisions for increased accuracy were made in situations where it was believed useful such as an increased number of mesh points between the bubble and the plate and integration of the plate

equation over an interval smaller than the fluid mesh spacing. Due to the finite time step size, the peak in the rigid system pressure history will be missed unless it occurs at a time step. For the 0.2 cm plate system model, this leads to an underestimation of the input rigid base plate pressure peak by about 2 1/2%.

6 Conclusions

The perturbation method is a promising practical tool for modeling FSI problems involving complex hydrodynamic transients. It allows the use of both experimental and analytical data from rigid systems subjected to identical hydrodynamic transients. The implementation of the perturbation method is much easier than alternate approaches which involve the simultaneous solution of the nonlinear hydrodynamic equations and the structural equations.

Our analytical and experimental investigation of FSI phenomena in a simple test system of controlled flexibility has demonstrated the important effects that liquid mass redistribution has on both the frequency content and the spatial and temporal amplitude distributions of the perturbation pressures.

REFERENCES

1 Huber, P.W., Kalumuck, K.M., and Sonin, A.A., "A Perturbation Method for Analyzing Fluid - Structure Interactions in Flexible Containers Partially Filled with Liquid," (previous paper).

2 Huber, P.W. and Javadi, Y.B., "Fluid-Structure Interactions in Pressure-Suppression Pools: Small-Scale Experiments," Nuclear Regulatory Commission Report NUREG/CR-0978, September 1979.

3 Sonin, A.A. and Huber, P.W., "On the Scaling Laws for Air Clearing in Water-Type Pressure Suppression Systems," Journal of Heat Transfer, Vol. 100, No. 4, 1978, pp. 601-604.

4 Anderson, W.G., Huber, P.W., and Sonin, A.A., "Experimental Tests of the Scaling Laws for Air Clearing in Water-Type Pressure Suppression Systems," Journal of Heat Transfer, Vol. 100, No. 4, 1978, pp. 605-612.

5 Timoshenko, S. and Woinowsky-Krieger, S., Theory of Plates and Shells, McGraw-Hill, New York, 1959, pp. 63-67.

6 Weber, C., "Calculation of Potential Fields and Electron Trajectories Using an Electronic Computer," Philips Technical Review, Vol. 24, No. 4/5, 1962/63, pp. 130-143.

7 Kalumuck, K.M., Engineer's Degree Thesis, M.I.T. Department of Mechanical Engineering, September, 1979.

8 Den Hartog, J.P., Advanced Strength of Materials, McGraw-Hill, New York, 1952, Chapter 4.

Table 1 Comparison of predicted flexible system sidewall pressure histories with experiment at z/a = 0.7

	0.1cm base plate		0.2cm base plate	
	prediction	experiment	prediction	experiment
$\frac{(P_p+P_R)_{max}}{(P_R)_{max}}$	0.98	1.21	1.06	1.06
Frequency (Hz)				
average	95[1]	135[1]	250[2]	295[2]
low (single cycle)	90	125	220	275
high (single cycle)	110	145	265	320
Decay rate[3]				
peak to peak	0.35	0.37	0.18	0.23
trough to trough	0.15	0.39	0.18	0.23

[1] Averaged over the first 7 cycles (beginning with the first peak in flexible system pressure occurring after $(P_R)_{max}$)

[2] Averaged over the first 12 cycles

[3] Computed from equation (18). The first 4 cycles are used for h=0.1cm; the first 10 cycles are used for h=0.2cm.

Table 2 Evaluation of perturbation method criteria for our test system

Characteristic and physical quantities:

L_w	0.08cm(1) 0.01cm(2)	L_g	14 cm	ρ_ℓ	1000 kg/m^3
L_R	14 cm	τ_R	0.04 s	ρ_g	0.08 kg/m^3(3)
L_λ	14 cm	τ_e	0.007 s	μ	0.001 kg/ms
L_0	14 cm	τ_w	0.01 s(1) 0.0035(2)	c_ℓ	1500 m/s
				c_g	330 m/s

	Criterion(4)	Value for test system	
		0.1 cm plate	0.2 cm plate
1)	$\tau_w/\tau_R \ll 1$	0.25	0.09
2)	$\frac{\tau_w}{\tau_R}\frac{L_R}{L_\lambda} \ll 1$	0.25	0.09
3)	$\tau_e/\tau_w \lesssim 1$	0.7	2
4)	$L_w/L_\lambda \ll 1$	0.006	0.0007
5)	$L_w/L_0 \ll 1$	0.006	0.0007
6)	$L_w/L_g \ll 1$	0.006	0.0007
7)	$(L_0/c_\ell\tau_w)^2 \ll 1$	0.00009	0.0007
8)	$(L_\lambda/c_\ell\tau_w)^2 \ll 1$	0.00009	0.0007
9)	$(L_g/c_g\tau_w)^2 \ll 1$	0.002	0.015
10)	$\rho_\ell L_\lambda^2/\mu\tau_w \gg 1$	2,000,000	5,600,000
11)	$\rho_g L_g/\rho_\ell L_0 \ll 1$	0.00008	0.00008

---

1 For a 0.1 cm base plate

2 For a 0.2 cm base plate

3 Based on an initial gas (air) pressure of approximately 6 kPa

4 Taken from [1]

LIST OF FIGURES

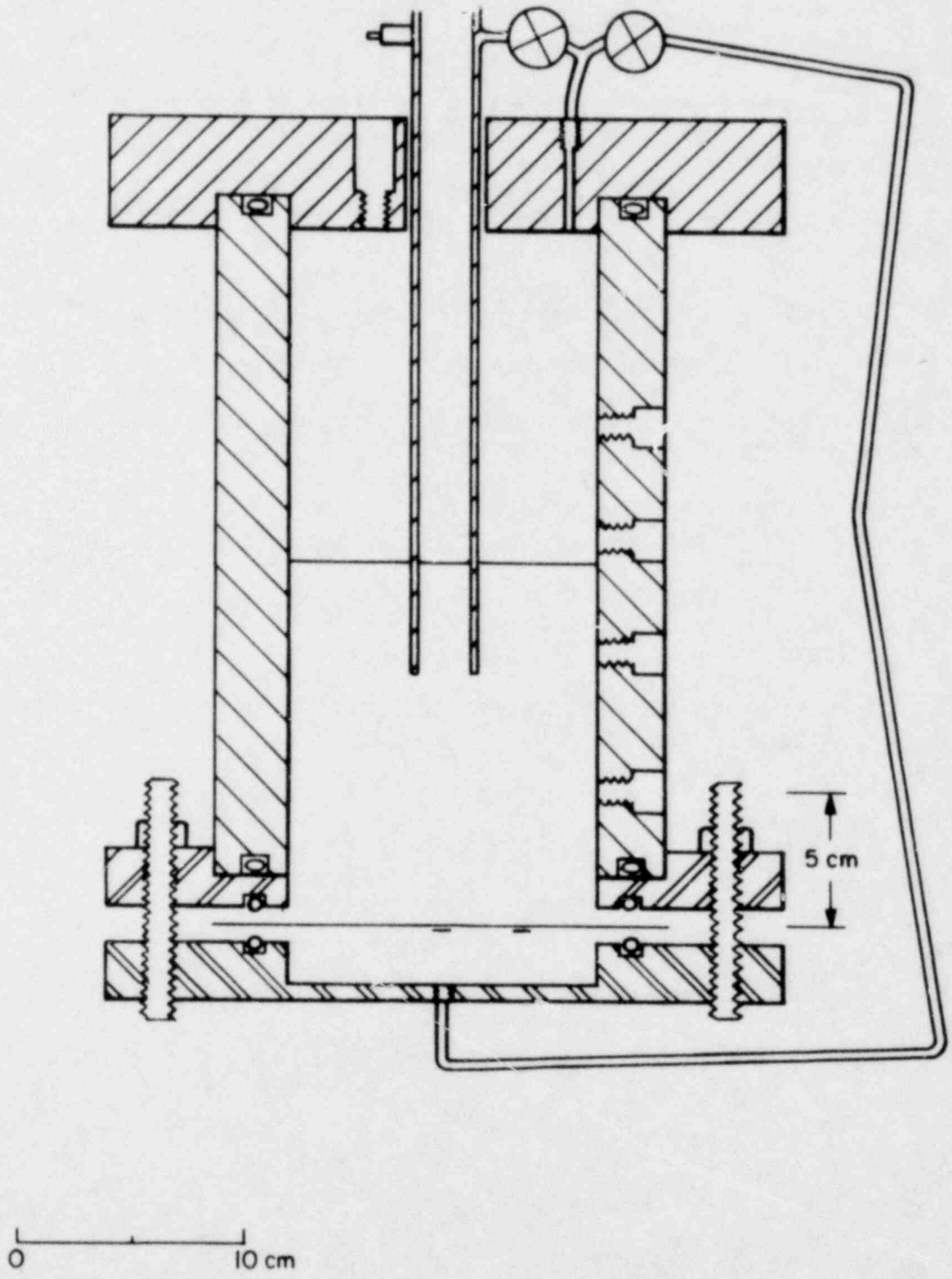

Figure 1 Schematic of test system

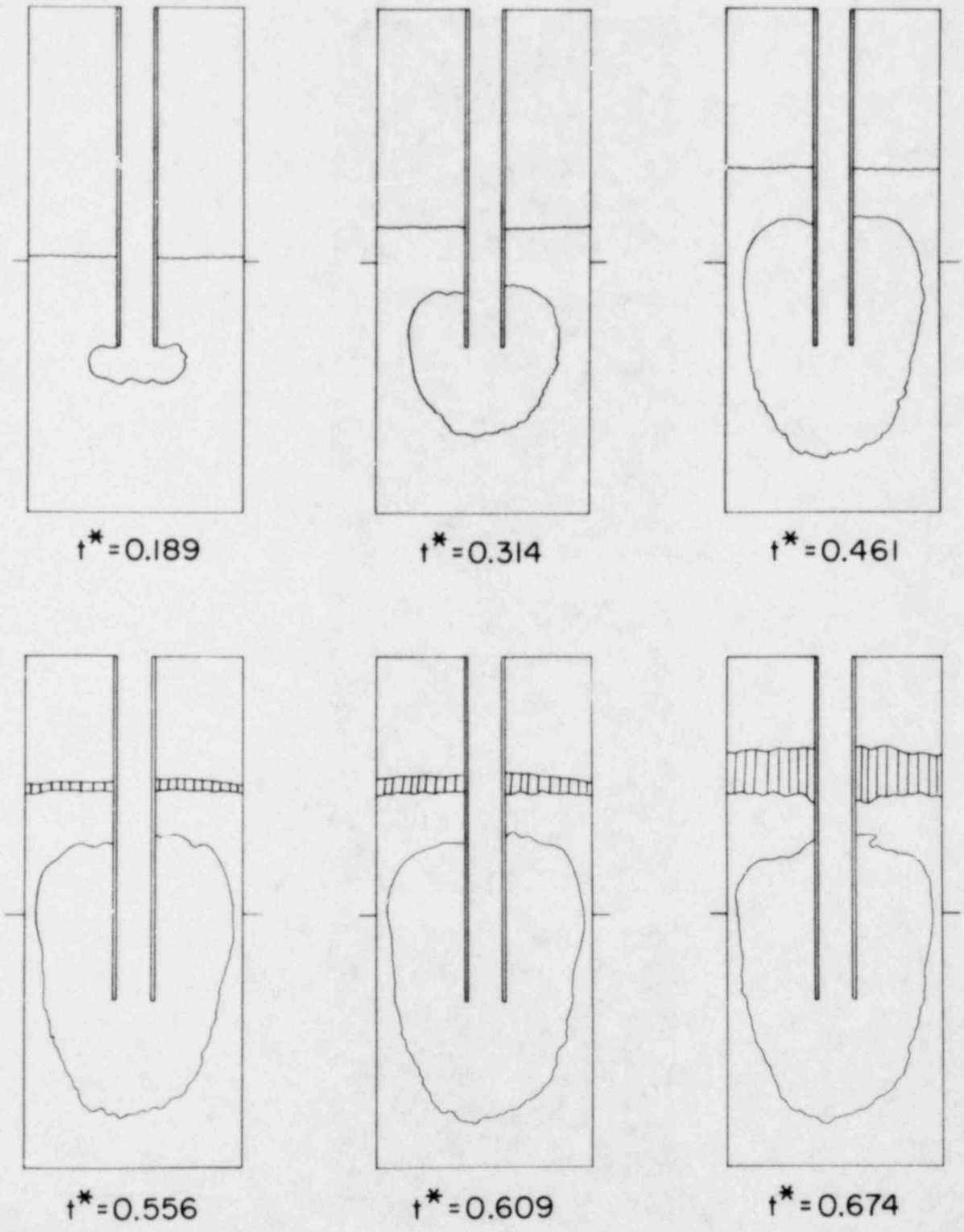

Figure 2 Pool swell history traced from high speed films. Hatch marks indicate growth of interface instability.

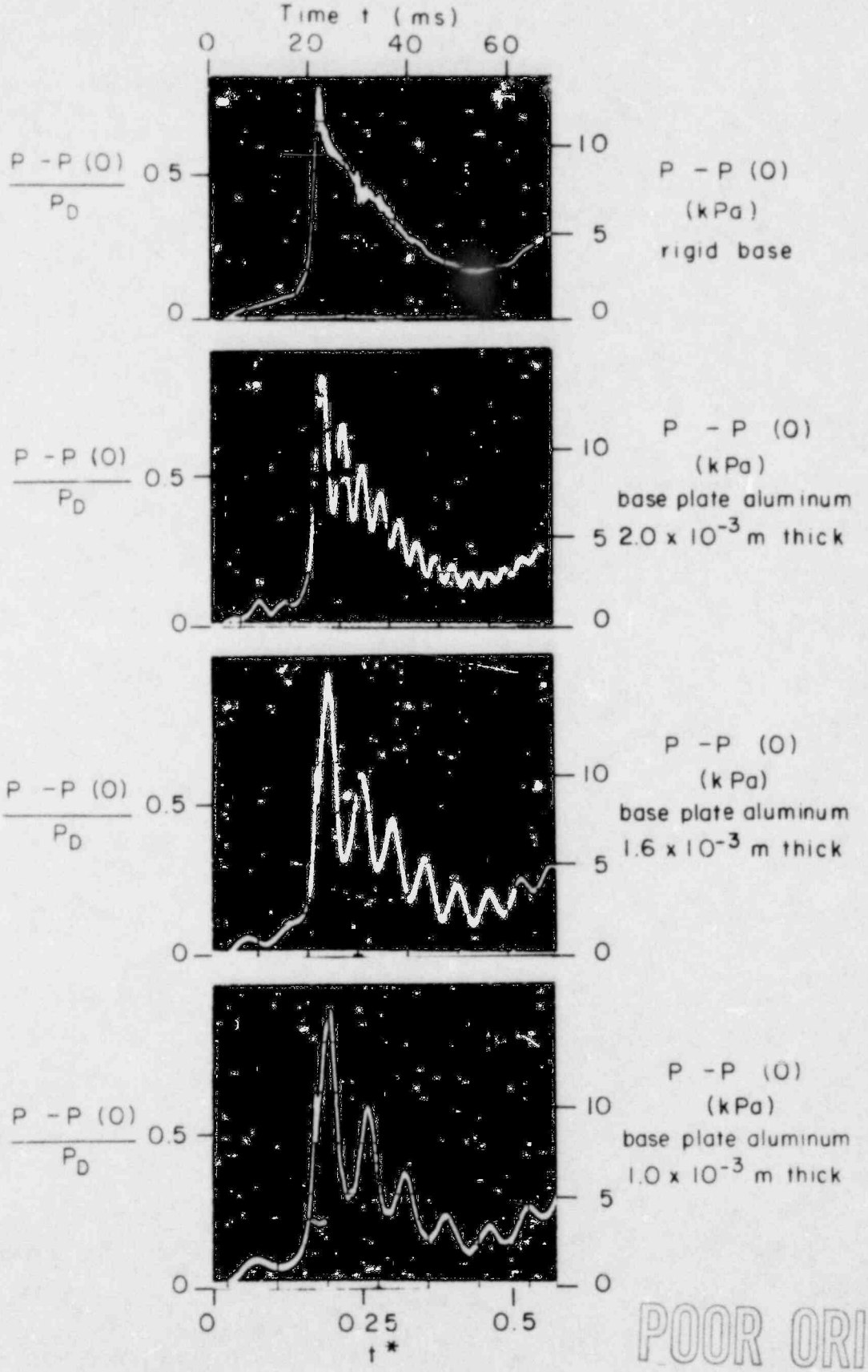

Figure 3 Experimental pressure histories on pool sidewall 5 cm above the base plate (z/a = 0.7)

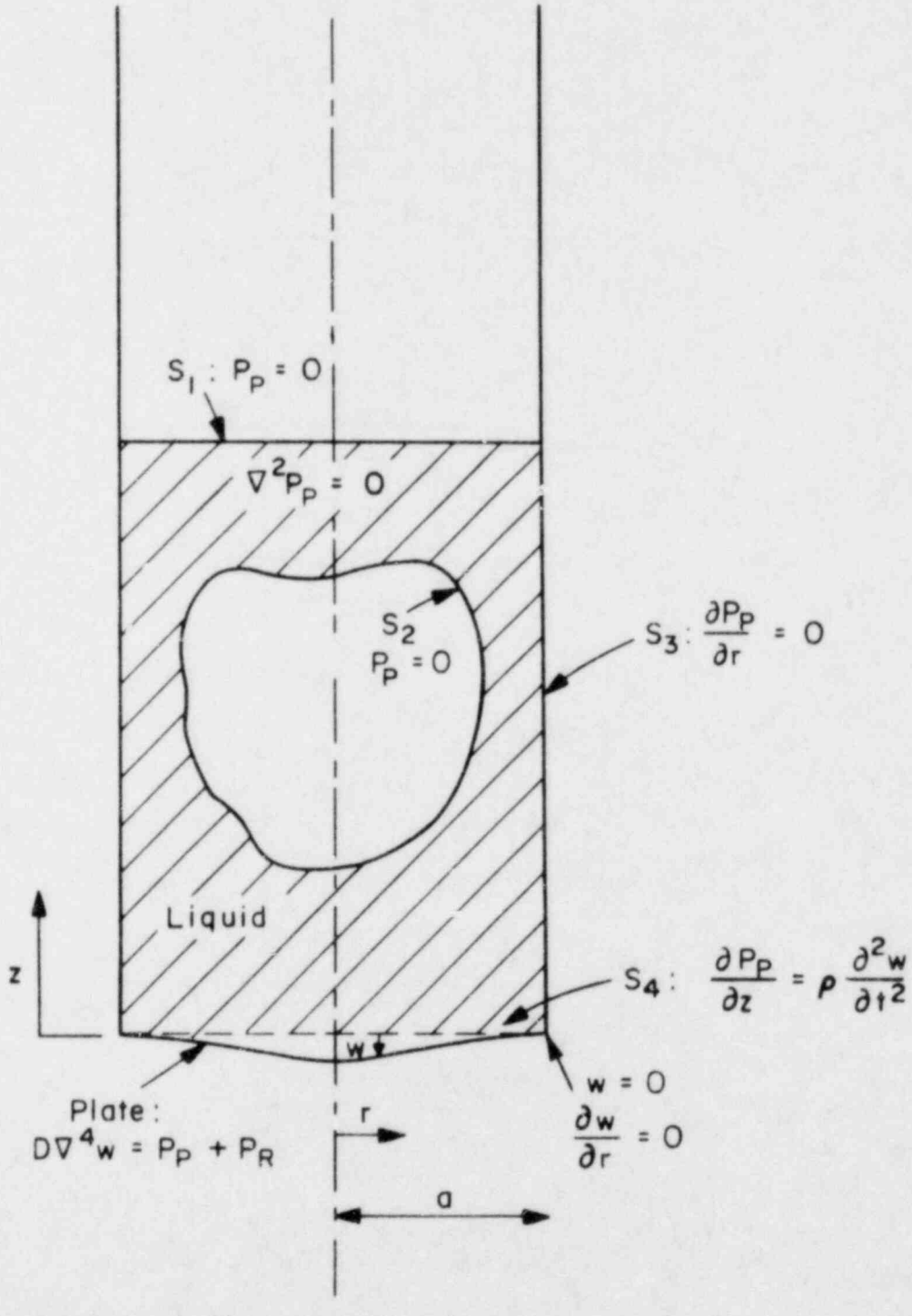

Figure 4 Equations and boundary conditions for perturbation calculation

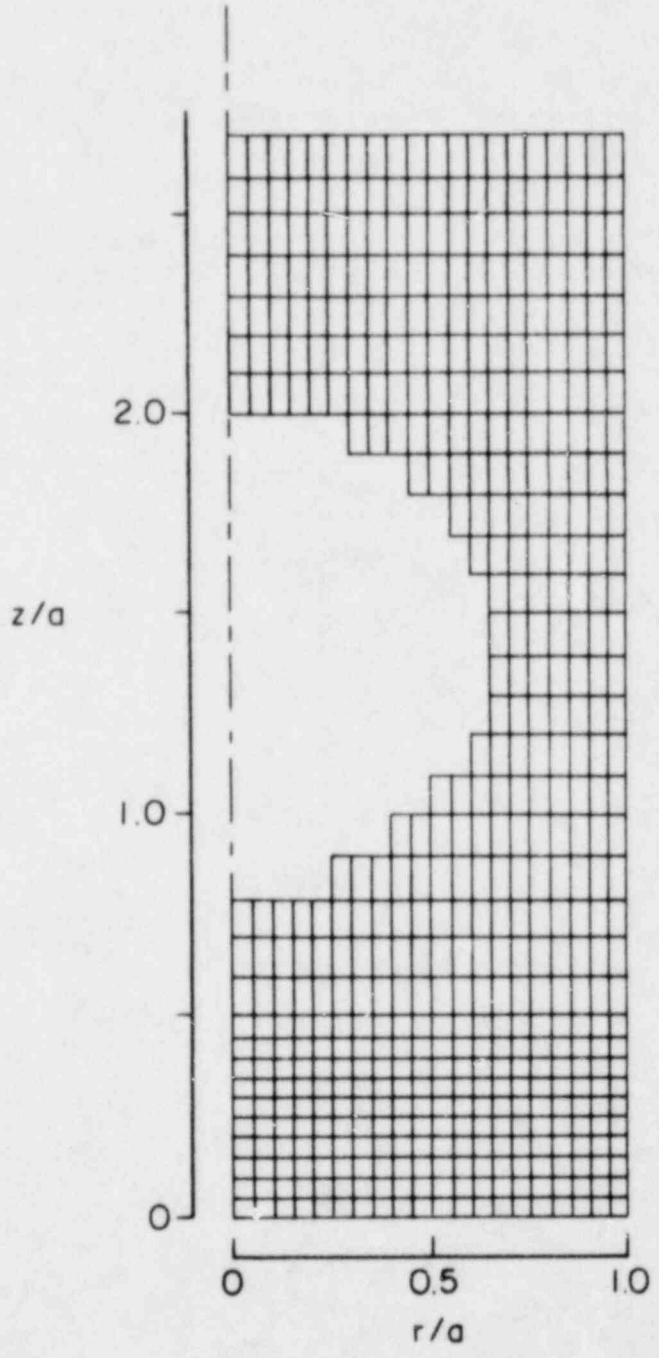

Figure 5 Typical fluid domain computation mesh (here for $t^* = 0.314$)

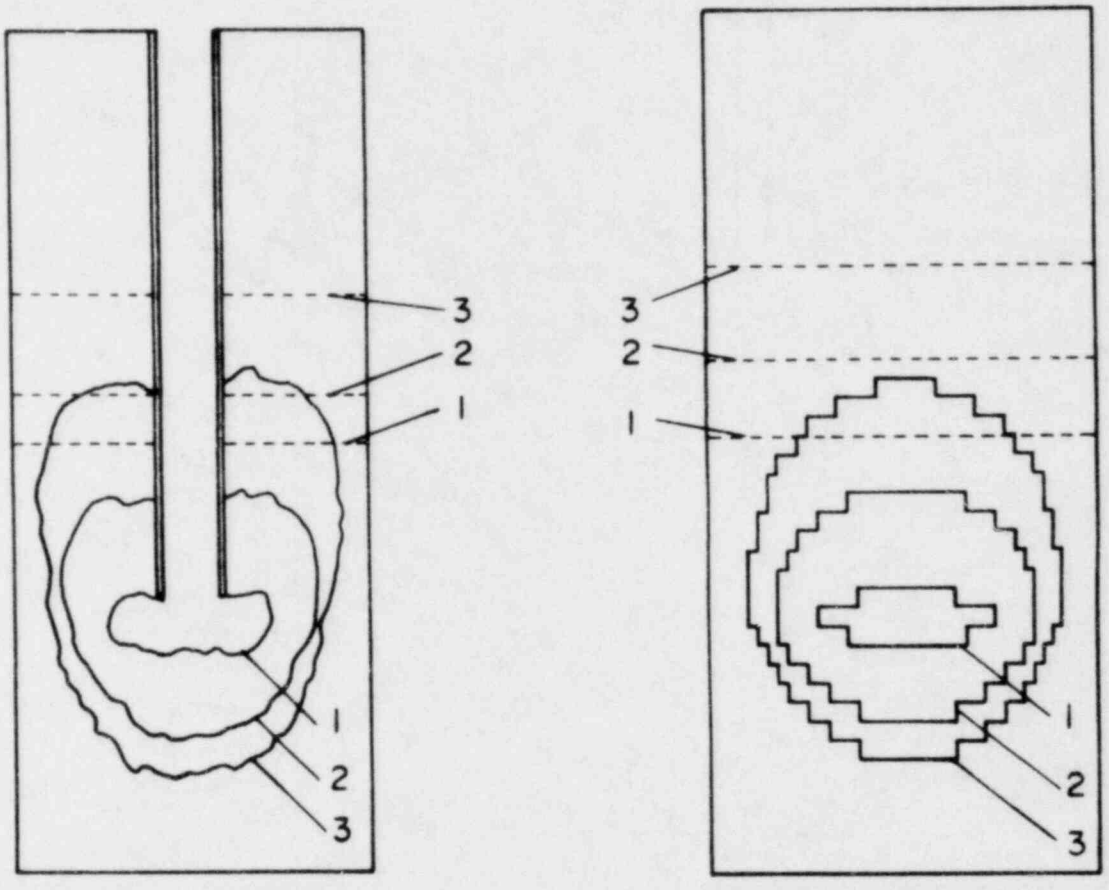

configuration	time (t^*)
1	0.189
2	0.314
3	0.461

Figure 6 Experimentally observed liquid configurations and corresponding model inputs at three sample times

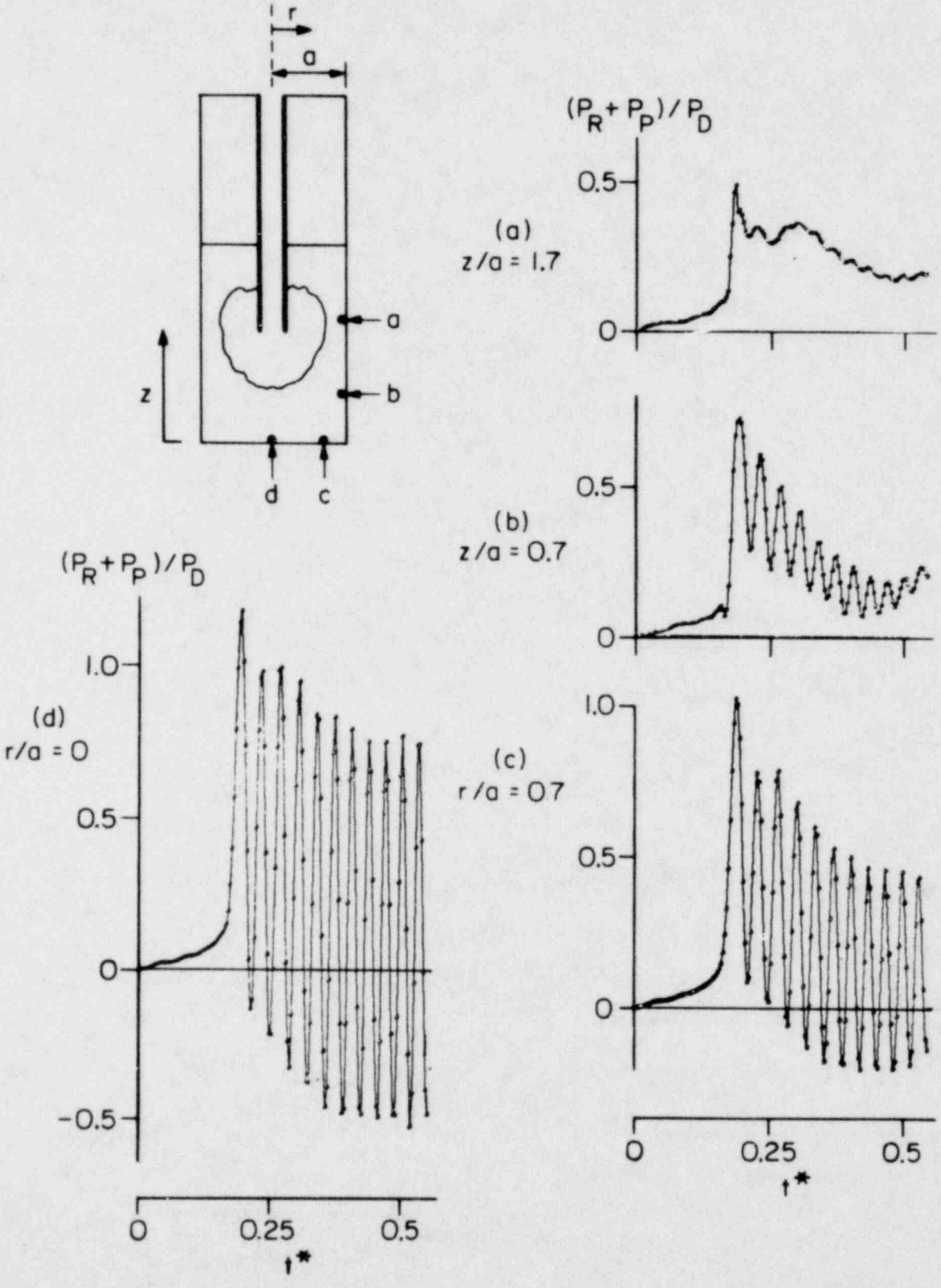

Figure 7 Model pressure history predictions for the 0.2 cm base plate. Calculated values are shown connected by straight lines.

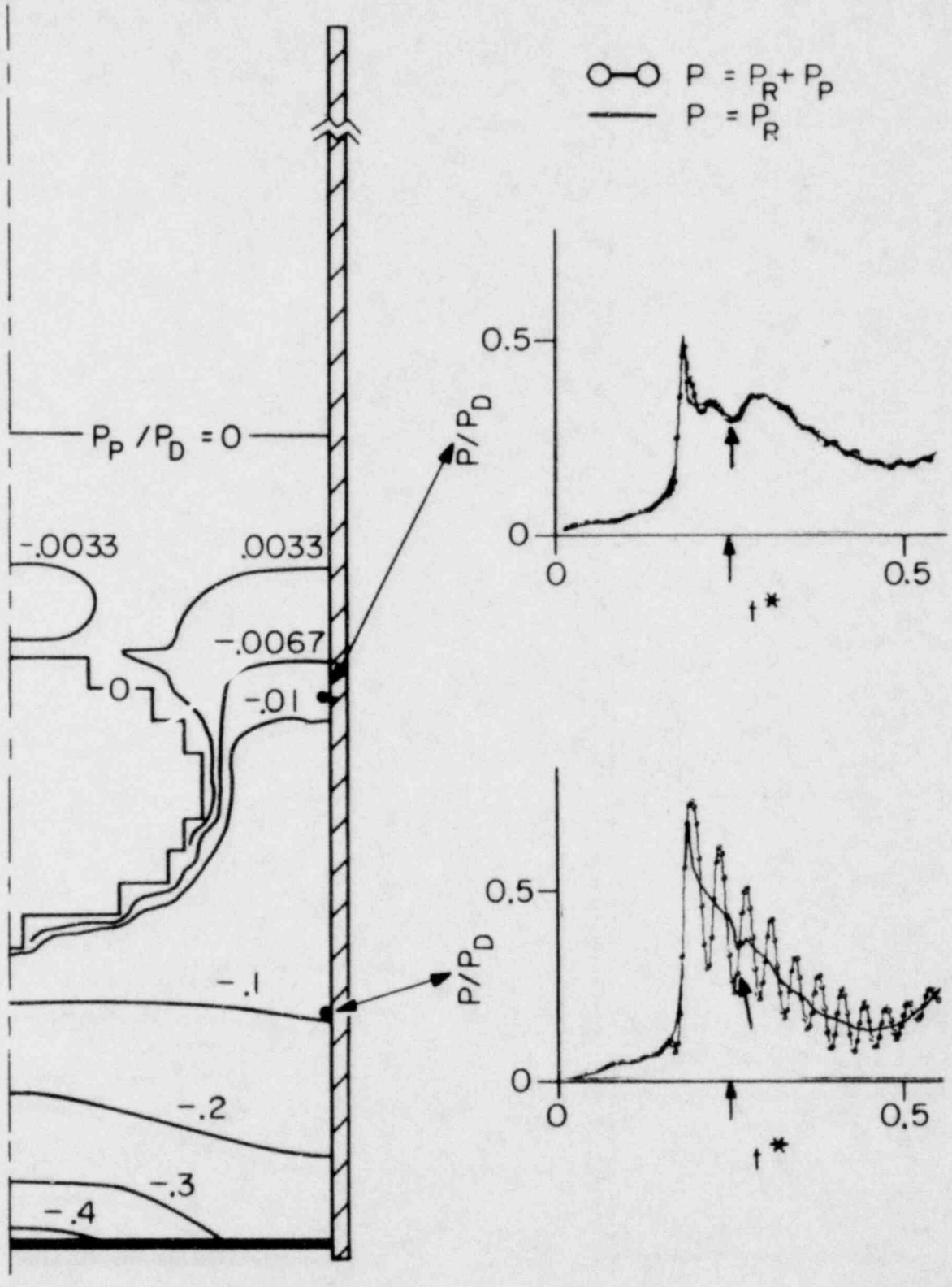

Figure 8 Predicted perturbation pressure field at t* = 0.249

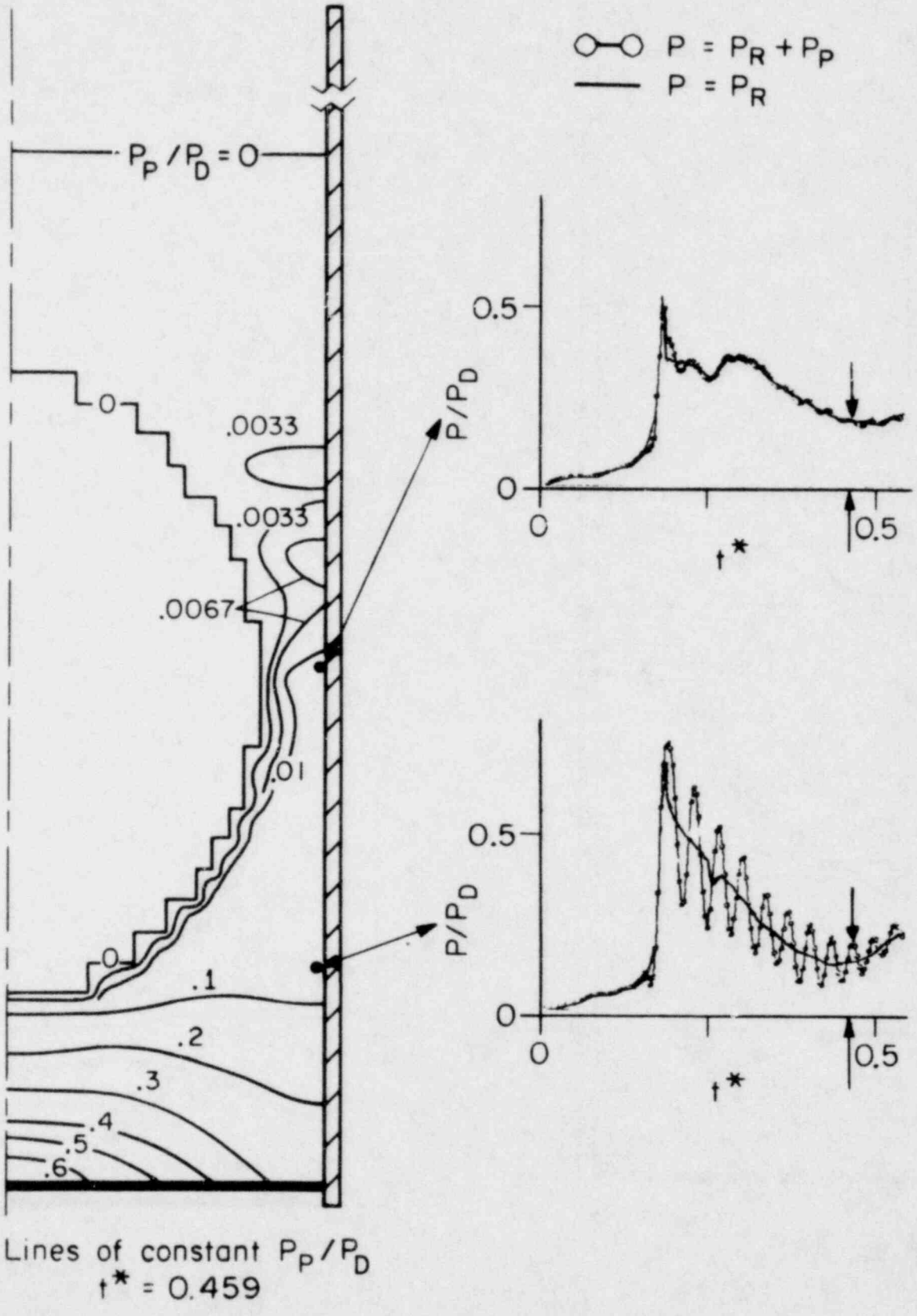

Figure 9 Predicted perturbation pressure field at t* = 0.459

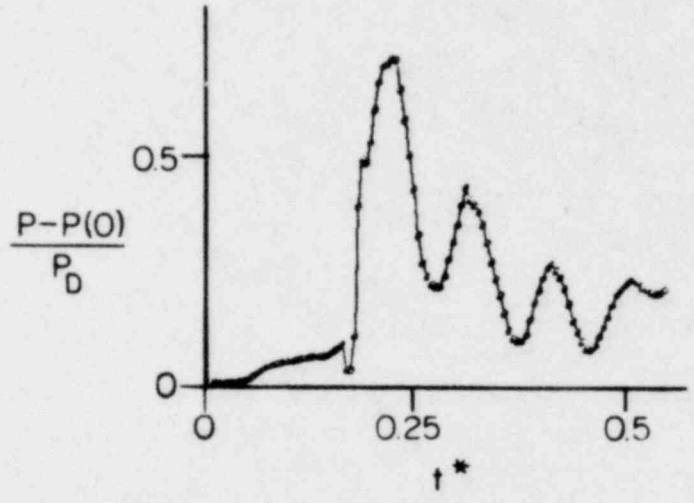

(a) Model prediction

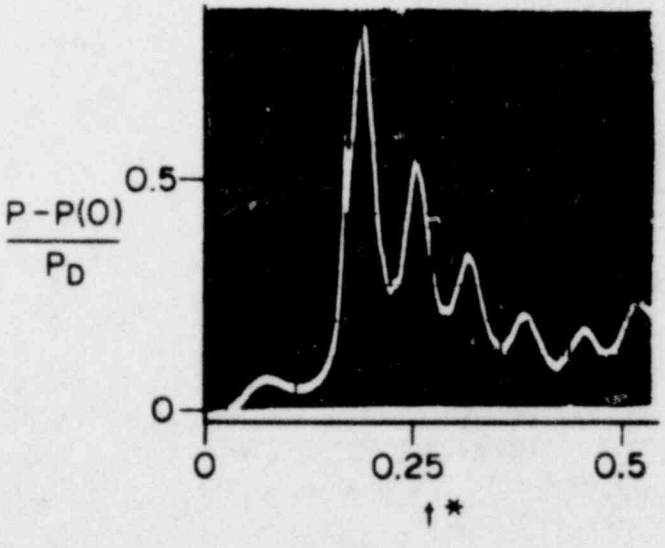

(b) Experiment

Figure 10 Comparison of sidewall perturbation calculation with experiment: 0.1 cm base plate, z/a = 0.7

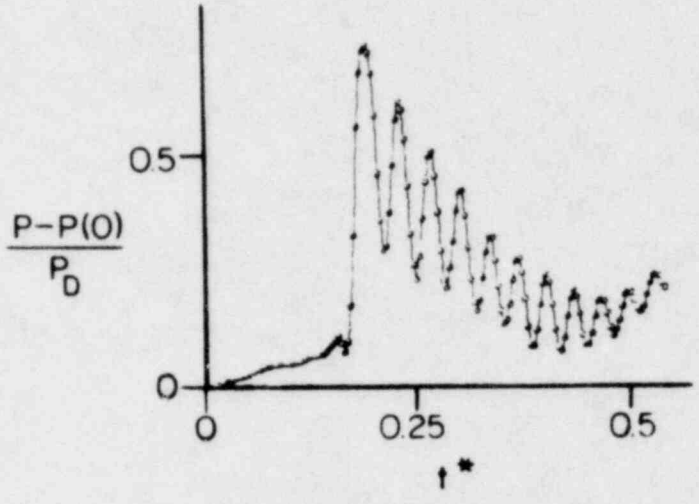

(a) Model prediction

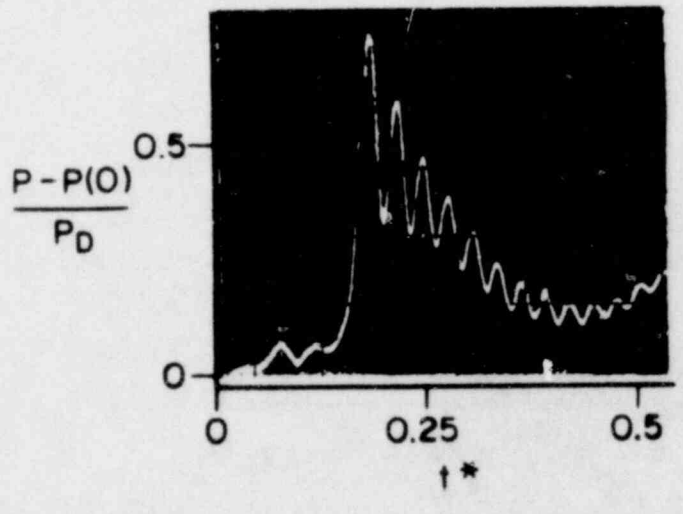

(b) Experiment

Figure 11 Comparison of sidewall perturbation calculation with experiment: 0.2 cm base plate, z/a = 0.7

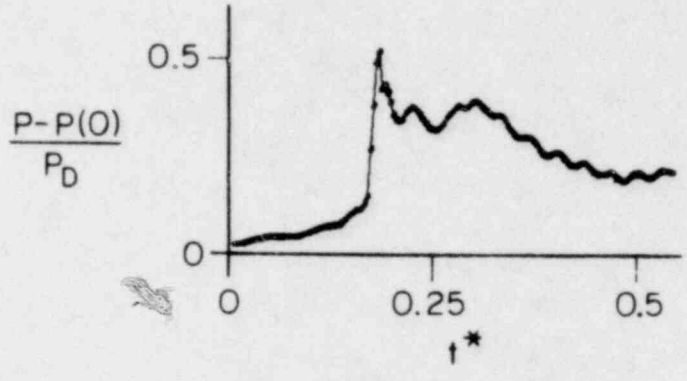

(a) Model prediction

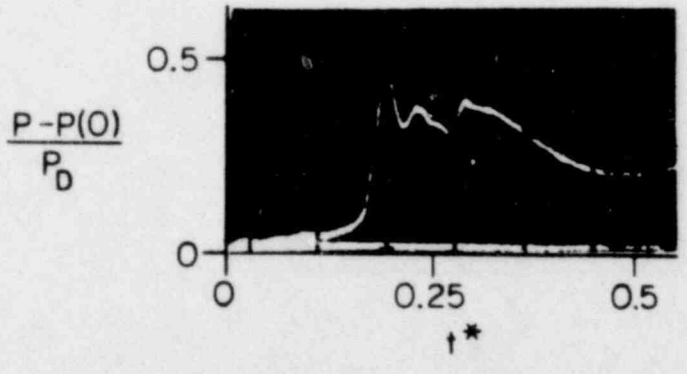

(b) Experiment

Figure 12 Comparison of sidewall perturbation calculation with experiment: 0.2 cm base plate, z/a = 1.7

NRC FORM 335 (7-77) U.S. NUCLEAR REGULATORY COMMISSION

BIBLIOGRAPHIC DATA SHEET

1. REPORT NUMBER (Assigned by DDC): CR-1313

4. TITLE AND SUBTITLE (Add Volume No., if appropriate): RATIONALE FOR A PERTURBATION METHOD FOR ANALYZING FLUID-STRUCTURE INTERACTIONS IN BWR PRESSURE_SUPPRESSION CONTAINMENT SYSTEMS

2. (Leave blank)

3. RECIPIENT'S ACCESSION NO.

7. AUTHOR(S): P. W. Huber, K. M. Kalumuck, A. A. Sonin

5. DATE REPORT COMPLETED: MONTH January, YEAR 1980

9. PERFORMING ORGANIZATION NAME AND MAILING ADDRESS (Include Zip Code):
Massachusetts Institute of Technology
Department of Mechanical Engineering
Cambridge, Mass 02139

DATE REPORT ISSUED: MONTH January, YEAR 1980

6. (Leave blank)

8. (Leave blank)

12. SPONSORING ORGANIZATION NAME AND MAILING ADDRESS (Include Zip Code):
Analysis Development Branch
Division of Reactor Safety Research
Office of Nuclear Regulatory Research
Washington, D. C. 20555

10. PROJECT/TASK/WORK UNIT NO.

11. CONTRACT NO.: NRC-04-77-011

13. TYPE OF REPORT: Topical Report

PERIOD COVERED (Inclusive dates):

15. SUPPLEMENTARY NOTES

14. (Leave blank)

16. ABSTRACT (200 words or less)

A formal justification is developed for a method in which hydrodynamic data for a transient in a rigid-wall system (derived, for example, from a small-scale experimental simulation) is used as input in a linear computation for the perturbation flow field due to actual wall flexibility. The method is useful in problems where the basic flow transient is so complex that it can be quantified only empirically, and where the fluid-structure interaction is too complex for the fluid side to be represented by a priori defined equivalent mass.

17. KEY WORDS AND DOCUMENT ANALYSIS

17a. DESCRIPTORS

17b. IDENTIFIERS/OPEN-ENDED TERMS

18. AVAILABILITY STATEMENT: Unlimited

19. SECURITY CLASS (This report): Unclassified

21. NO. OF PAGES

20. SECURITY CLASS (This page)

22. PRICE: $